# THE EFFECTS OF INITIAL CONDITION OF FRACTURE SURFACES, ACID SPENDING, AND TYPE ON CONDUCTIVITY OF ACID FRACTURE

A Thesis

by

ALI MANSOUR A. ALMOMEN

Submitted to the Office of Graduate Studies of
Texas A&M University
in partial fulfillment of the requirements for the degree of

MASTER OF SCIENCE

| | |
|---|---|
| Chair of Committee, | Ding Zhu |
| Committee Members, | A. Daniel Hill |
| | Yuefeng Sun |
| Head of Department, | A. Daniel Hill |

August 2013

Major Subject: Petroleum Engineering

## ABSTRACT

Fracture conductivity and the effects of treatment variables can be studied in the laboratory. We conducted experiments based on scaling down the field conditions to laboratory scale by matching Reynold's and Peclet numbers. Experiments conducted were comprised of three stages: dynamic etching, surface characterization of etched cores, and conductivity measurement. The effect of initial condition of fracture surfaces on the etching pattern and conductivity were investigated in this study. Another area of interest is the variation of conductivity along the fracture due to acid spending. We also investigated the contact time, acid system type, and treatment temperature effects on conductivity using San Andres dolomite cores.

The results from these studies showed that rough-surface fractures generate higher conductivity by an order of magnitude compared with a smooth-surface fracture at low-closure stress. Also, conductivity generated on rough-surface fractures by smoothing peaks and deepening valleys which widen the gap between the fracture surfaces after closure and acid creates conductivity on smooth-surface fractures by differential etching that creates asperities.

The results suggest that an increase in acid spending does not automatically result in lower conductivity; and etched volume alone is not adequate to predicate the conductivity. Conductivity results from a combination of etching pattern, etched volume, and rock compressive strength after etching.

In-situ crosslinked acid was found to be more effective in etching rock and controlling acid leakoff compared with linear-gelled acid. Also, crosslinked acid reduces the number of pits and the pit diameters. Based on conductivity tests, linear-gelled acid is more favorable at higher temperatures while in-situ crosslinked acid showed higher conductivity at lower temperatures. For a rough-surface fracture, shorter contact time created high conductivity compared to longer contact while injecting the same volume of acid, suggesting the existence of an optimum contact time.

## DEDICATION

To Lujain and my parents

## ACKNOWLEDGMENTS

I would like to take this opportunity to thank my advisors Dr. Ding Zhu and Dr. Dan Hill for their guidance, support and patience throughout the course of this study. Also, I would like to acknowledge Dr. Yuefeng Sun for serving as committee member.

Special thanks to acid fracturing team members: Andrea Nino Penaloza, Jarrod Underwood and Murtada Aljawad for their help and support in running experiments and undergrad student worker Rongqiang Chen for his effort in preparing cores and helping with conductivity experiments.

Finally, I would like to extend my gratitude to the Crisman Institute at the Department of Petroleum Engineering at Texas A&M University for funding the research project.

# TABLE OF CONTENTS

Page

## LIST OF FIGURES

Page

## LIST OF TABLES

# 1 INTRODUCTION

## 1.1 Statement of the Problem

Acid fracturing is a stimulation technique in which acid is injected into a formation at a pressure greater than the rock fracturing pressure, resulting in tensile failure of the rock. The injected acid reacts with the fracture faces in a nonuniform pattern, creating a conductive path for the reservoir fluid after the injection has stopped and the fracture is allowed to close-up (Fig. 1).

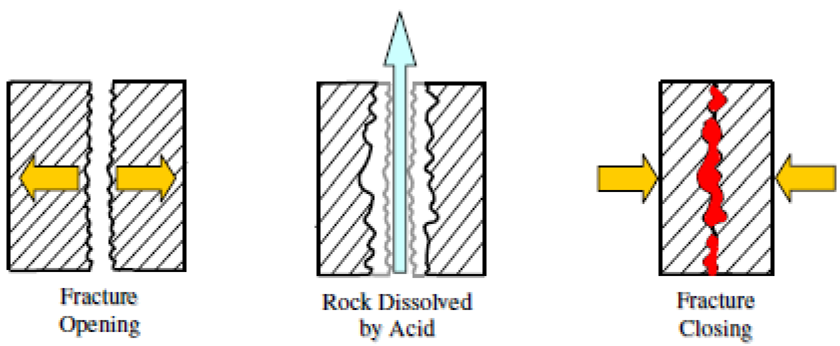


**Figure 1: Evolution of an acid fracture**

Often, a viscous pad fluid is injected ahead of the acid to increase the fracture width as well as to deposit a filter cake on the fracture surfaces. This condition helps to increase the distance the live acid travels along the fracture before it is entirely spent.

A successful acid-fracturing treatment design optimizes the effective fracture length in addition to the fracture conductivity, and maximizes the well productivity.

Predicting the conductivity of an acid fracture using theoretical models is challenging due to the stochastic nature of the acid reaction with rock along with the complex leakoff behavior of acid. Conductivity is predicted using empirical correlations relating fracture conductivity with parameters such as volume of rock dissolved, closure stress of formation, rock mechanical strength, roughness, and etching pattern.

The correlations presented in the literature all use the same parameters that are evaluated from experiments. However, there are uncertainties in estimating these parameters. These uncertainties are attributed to the source of core samples, which mainly come from quarried rocks, repeatability of experiments, proper scaling of laboratory conditions to represent field conditions, and core sample sizes.

The mechanism for creating conductivity in an acid-fracturing treatment is a controversial subject. Many investigators suggest that acid creates asperities, which act as pillars that hold the fracture open. Other investigators believe that acid smoothes the peaks and valleys created by the pad fluid, which creates a mismatch between the fracture surfaces, resulting in a conductive path for the reservoir fluid. To better understand the conductivity creation mechanism, the effects that the initial condition of fracture surfaces have on etching pattern and conductivity need to be investigated by running a comparative study between smooth- and rough-surface fractures.

A shortcoming of previous works is that these experiments only represent the entrance of a fracture when it is exposed to a live acid. Experiments at different stages of acid spending need to be investigated to understand how conductivity varies along an acid fracture.

The cooling effect acid has when designing experimental conditions is a drawback of previous works addressed in this study. Previously, experiments were run at reservoir temperature rather than treatment temperature.

The effects resulting from treatment temperature, acid system type, and contact time on the etching pattern and conductivity of rough-surfaces of San Andres dolomite cores were also studied in this work.

## 1.2 Literature Review

### 1.2.1 Experimental work

Numerous investigators have attempted to understand acid-fracture conductivity by designing an experimental setup to capture the majority of the characteristics of field treatments. Many of these experiments focused on understanding the effect of treatment variables on fracture conductivity such as pumping rate, temperature, acid system type, and contact time. Others were interested in correlating conductivity with parameters such as rock mechanical strength and the volume of rock dissolved. A brief description of the previous investigations is provided in this section

Barron et al. (1962) studied the relationship between reaction rate of HCl acid and its shear rate. They estimated the spending time and penetration distance of an acid in a fracture and also developed an equation relating injection rate, fracture width, acid concentration, contact time, and fracture height for both linear and radial fracture systems. They concluded that the time spent by acid in a fracture depends on the reaction rate, which depends on temperature, pressure, acid concentration, rock composition, and the ratio of the acid volume to the surface area of the rock.

To predict the stimulation ratio of an acid-fracturing treatment, Nierode et al. (1972) developed a procedure coupling a theoretical model for the acid reaction during its flow along a fracture with experimentally determined rate of acid transfer to the fracture walls. They studied the effects on the stimulation ratio brought about by injection rate, temperature, width created by pad fluid, and acid concentration. The results of their study found that by increasing the injection rate, fracture width created by pad fluid and acid concentration increases penetration distance while an increase in temperature decreases acid penetration due to a decrease in viscosity and an increase in mixing coefficient

Nierode and Kruk (1973) correlated fracture conductivity with dissolved rock equivalent conductivity (DREC), rock strength measured by rock embedment strength (RES), and closure stress ($\sigma_c$). They concluded that for smoothed surfaces, fracture conductivity is generated due to heterogeneities of the rock while for homogenous formations, the conductivity resulting from smoothening peaks and valleys can generate highly conductive fractures. These results suggested that conductivity measured in their tests is mainly due to the smoothing of peaks and valleys on the rough surface and is independent of rock heterogeneities due to their small size. Their predictions showed that when RES is very low, the points of support on fracture surfaces will collapse, and the resulting fracture will have low conductivity, whereas high conductivity in the range of $10^5$ to $10^7$ md-inches is obtained when RES is high.

Crowe (1981) evaluated various types of polymers and thickening agents as gelling agents for HCl acid. He employed three criteria to compare these materials: thickening efficiency, acid stability, and residue formation.

Anderson and Fredrickson (1989) concluded that two parameters determine conductivity of acid fracture: the amount of rock dissolved and the pattern of rock removal. They stated that formation characteristics dominate conductivity generated from the acidizing process and the mineralogical composition of a formation is likely the most important factor because the etching pattern directly depends on the degree of homogeneities. Also, the variation of permeability and porosity affects the etching pattern and fluid leakoff depends on those properties. They also found that the magnitude of the conductivity reduction is a function of the rock strength and the ratio of supporting area to etched area.

The effect on conductivity by acid leakoff into the formation was studied by Malik and Hill (1989). Their results showed that the trends of conductivity with stress for limestone core samples etched with acid, both with and without leakoff, were similar except that a sharp drop was observed for the case with no leakoff at high closure stress.

Anderson (1991) investigated the difference in reactivity data generated by quarried samples and actual formation cores using San Andres dolomite cores.

Predicating etched fracture conductivity and effective fracture length influenced by acid spending and leakoff of reactive fluids were investigated by Van Domelen (1992). She found that the surface reaction rate of many formations is much less than the rate predicated in the laboratory because laboratory results are based on quarried rocks and fluid leakoff characteristics measured in the field are significantly greater than those measured in the laboratory. She concluded that fluid leakoff is the primary cause for limited effective fracture length, and the fluid loss coefficient is for the most part related to initial permeability.

Van Domelen et al. (1994) described the design aspect of acid fracturing in high-temperature/high-closure stress reservoirs and used cores to evaluate the reactivity of the formation and to characterize etching characteristics. They suggested that the relative difference between zero-closure stress conductivity and conductivities at higher closure stress provides a quantitative indication of the degree of differential etching.

One of the studies addressing the effect of contact time and fluid loss on generated conductivity for different types of rock was conducted by Beg et al. (1996). In their work, fluid was allowed to leak off as a portion of the total flow rate. They showed that acid-fracture conductivity is occasionally reduced with longer contact time due to the weakening of the rock. Also, an optimum contact time may exist in acid fracturing because either too little or too much dissolution may result in lower conductivity. Based on their results, higher fracture conductivity results when a fluid is allowed to leak into cores than for the case with no leakoff.

Gong et al. (1998) also investigated the effects of contact time and acid leakoff on created conductivity. They found that as contact time increases, the height distribution of asperities grows wider, and the longer the contact time, the rougher the fracture surface; hence, the higher the conductivity. They showed that hardness of acidized cores was typically less than that of nonacidized cores. Also, the initial conductivity tended to increase with increasing contact time, whereas leakoff of acid does not have a consistent effect on conductivity.

Abass et al. (2006) studied the effects that elastic, plastic, and creeping deformations have in reducing fracture conductivity. Their work focused on the rock mechanics aspect of fracture closure, and they employed a creeping test to provide an additional criterion for use in selecting between proppant and acid fracturing. They suggested that productivity decreases in acid-fractured well is an integrated effect of elastic, plastic, and creeping responses to applied stress.

The role of rock strength reduction of limestone and dolomite formations due to acid etching on conductivity of acid fractures was addressed by Nasr-El-Din et al. (2006). They determined that softening of rock samples is a function of formation permeability and leakoff of live or partially spent acid into the matrix and softening effect on limestone is greater than on dolomite even for higher permeability dolomite samples. Also, they found that straight acid softens limestone from 1.42 to 11.04 and dolomite 2.75 to 25.6 times as much as gelled and emulsified acid. Their work showed that when gelled acid was used where viscosity controls the leakoff, less strength reduction was observed.

Proper down scaling of field conditions to accurately represent laboratory conditions was addressed by Pournik (2008). To match field conditions with laboratory conditions, Reynold's number was used to represent the flow along the fracture faces as well as acid leakoff into the fracture faces, and Pecelt number was used to represent acid transport to the walls of a facture.

Antelo et al. (2009) suggested that conductivity is a function of the amount of rock dissolved, which is controlled by kinetic parameters and the mineralogical composition along with the degree of heterogeneity of the rock. They observed three different etching patterns: channeling, roughness, and cavity.

The feasibility of acid fracturing of hard- and deep-limestone reservoirs was addressed by Neumann et al. (2012a) in which they concluded that acid fractures can exist in carbonate reservoirs with closure stress greater than 5000 psi. To characterize fracture surfaces, they used the linear roughness parameter defined as actual surface area to projected surface area and introduced a graphic criterion to determine the feasibility of acid fracturing called the acid-fracturing conductivity window.

In a different study, Neumann et al. (2012b) discussed the asperities paradigm in which they showed the difference between rocks with wet sawed fracture surfaces and tensile fracture surfaces. To characterize fracture surfaces, they used two parameters, linear roughness and tensile linear roughness which is defined as the actual area of the fracture surface before acid etching to the actual area after acid etching. They concluded that surfaces of tensile fractures after acid etching can be smoother, rougher, or remain the same.

### 1.2.2 Conductivity predication

Nierode and Kruck (1973) were among the pioneers attempting to empirically model the conductivity of acid fracture. The essence of their correlation was to predict the conductivity of a fracture under zero-closure stress, assuming that the acid would dissolve the surfaces of a fracture in a uniform pattern, creating a fracture with a constant width known as the ideal fracture width ($w_i$). They correlated $w_i$ with the measured fracture conductivity, RES, and closure stress ($\sigma_c$). RES is defined as the force required to push a steel ball bearing into a rock surface to a distance equal to the radius of the ball divided by the projected area of the bearing. Their correlation is shown below:

$$k_f\,w = C_1 \exp(-C_2\sigma_c)$$

$$C_1 = \left(k_f\,w\right)_0 = 1.47\;x\;10^7 w_i^{2.47}$$

$$C_2 = (13.9 - 1.3\ln(RES))x\;10^{-3} for\;RES < 20{,}000\;psi$$

$$C_2 = (3.8 - 0.28\ln(RES))x\;10^{-3} for\;RES > 20{,}000\;psi$$

Walsh (1981) derived a model for conductivity of rough-surfaces fracture for laminar flow:

$$\left(k_f w\right) = \left(k_f w\right)_0 \left[1 - \left(\frac{\sqrt{2h}}{a_0}\right)\ln(\sigma_c - p_0)\right]\left[\frac{1 - b(\sigma_c - p_0)}{1 + b(\sigma_c - p_0)}\right]$$

$$b = \sqrt{3}\pi\left(\frac{f}{h}\right)E(1 - v^2)$$

where $p_0$ is reference pressure, $a_0$ is the half fracture width at some reference pressure, E is Young's modulus, $v$ is Poisson's ration, $f$ is the auto-correlation distance, and $h$ is the root mean square value of the height distribution.

Nasr-El-Din et al. (2006) indicated that the results of Nierode and Kruck (1973) were lumped together and did not differentiate between lithology.

They separated the correlation into two correlations based on lithology:

**The limestone correlation:**

$$k_f\,w = C_1 \exp(-C_2\sigma_c)$$

$$C_1 = \left(k_f\,w\right)_0 = 0.165\;DREC^{0.8746}$$

$$C_2 = (26.567 - 8.6341\ \ln(RES))x\ 10^{-3} for\ RES < 20{,}000\ psi$$

$$C_2 = (2.9795 - 0.202\ \ln(RES))x\ 10^{-3} for\ RES > 20{,}000\ psi$$

**The dolomite correlation:**

$$k_f\ w = C_1 \exp(-C_2\sigma_c)$$

$$C_1 = \left(k_f\ w\right)_0 = 13.29\ DREC^{0.5592}$$

$$C_2 = (8.6383 - 0.7479\ \ln(RES))x\ 10^{-3} for\ RES < 20{,}000\ psi$$

$$C_2 = (2.3147 - 0.1513 \ln(RES))x\ 10^{-3} for\ RES > 20{,}000\ psi$$

where $(k_f w)_0$ is the initial fracture conductivity under zero closure stress and *DREC* is the dissolved rock equivalent conductivity.

Gong et al. (1999) developed a model which considers both surface roughness and rock mechanical properties (fracture deformation model):

$$k_f w = (k_f w)_0 \left[1 - \left(\frac{4+K}{5+K}\right)\left(\frac{2\sigma_c}{c\ \sigma_y}\right)^{1/(K+4)}\right]^6$$

where *K* is the kurtosis of asperity height distribution, *c* is a stress correction factor and $\sigma_y$ is the rock yield stress.

Deng et al. (2012) developed conductivity correlations that consider permeability, mineralogy distribution, elastic properties of the rock, and fracture etching profile. They classified the etching pattern into three types based on the relative contribution of each of the factors considered in their study which are permeability dominant, mineralogy dominant, and combination effect of both. The correlations for each of the dominant effects are shown below.

**Permeability distribution dominant:**

$$wk_f = \alpha\ exp\ [-\beta\sigma_c]$$

$$\alpha = (k_f w)_0 \left[0.22(\lambda_{D,x}\sigma_D)^{2.8} + 0.011(\left(1 - \lambda_{D,z}\right)\sigma_D)^{0.4}\right]^{0.52}$$

$\beta = [14.9 - 3.78\, ln(\sigma_D) - 6.81\, ln(E)]x\ 10^{-4}$

$$(k_f w)_0 = 4.48 \times 10^9 \overline{w}^3 \left[1 + (a_1\ \mathrm{erf}\left(a_2\left(\lambda_{D,x} - a_3\right)\right) - a_4 \mathrm{erf}(a_5\left(\lambda_{D,z} - a_6\right)))\sqrt{e^{\sigma_D} - 1}\right]$$

$$a_1 = 1.82 \quad a_2 = 3.25 \quad a_3 = 0.12 \quad a_4 = 1.31 \quad a_5 = 6.71 \quad a_6 = 0.03$$

where $\lambda_{D,x}$ is the normalized horizontal length, $\lambda_{D,z}$ is the normalized vertical length, $\sigma_D$ is the normalized standard deviation, E is the Young's modulus, and w is the average fracture width.

**Mineralogy distribution dominant**

$wk_f = \alpha\ exp\ [-\beta\sigma_c]$

$\alpha = (k_f w)_0\ (0.811 - 0.853 f_{calcite})$

$\beta = [1.2 \exp(0.952\ f_{calcite}) - 10.5E^{-1.823}]x\ 10^{-4}$

$(k_f w)_0 = 4.48 \times 10^9 [1 + 2.97(1 - f_{calcite})^{2.02}\ ]\left[0.13\ f_{calcite}^{0.56}\right]^3 w_i^{2.52}$

where $f_{calcite}$ is the percentage of calcite.

**Competing effect of permeability and mineralogy:**

$wk_f = \alpha\ exp\ [-\beta\sigma_c]$

$\alpha = (k_f w)_0\ \left[0.21 {\lambda_{D,x}}^{0.16} + 0.046 \ln(\sigma_D) + {\lambda_{D,z}}^{-0.17}\ \right]$

$\beta = [53.8 - 4.58 \ln(E) + 18.9 \ln(\sigma_D]x\ 10^{-4}$

$$(k_f w)_0 = 4.48 \times 10^9 \left[1 + a_1 + (a_2\ \mathrm{erf}\left(a_3\left(\lambda_{D,x} - a_4\right)\right) - a_5 \mathrm{erf}(a_6\left(\lambda_{D,z} - a_7\right)))\sqrt{e^{\sigma_D} - 1}\right] \left[a_8 f_{calcite}^{a_9} + a_{10}\sigma_D\right]^3 w_i^{a_{11}}$$

$$a_1 = 0.2 \quad a_2 = 1.0 \quad a_3 = 5.0 \quad a_4 = 0.12 \quad a_5 = 0.6 \quad a_6 = 3.5 \quad a_7 = 0.03\ a_8 = 0.1 \quad a_9 = 0.43 \quad a_{10} = 0.14 \quad a_{11} = 2.52$$

## 1.3 Research Objective

The present study aims to achieve following objectives:

- Study the effect that the initial condition of fracture surfaces (rough- and smooth-surface) has on conductivity and etching pattern
- Study the effect that acid spending has as acid travels along the fracture on conductivity and etching pattern
- Study the effects that treatment temperature, acid system type, and contact time have on conductivity and etching pattern.
- Compare the experimental results with the N-K and Deng-Mou correlations.

# 2 EXPERIMENTAL APPARATUS, PROCEDURE, AND TESTING CONDITIONS

## 2.1 Experimental Apparatus Description

Experiments conducted in this study consist of three main stages: a dynamic etching test, surface characterization of cores, and a conductivity test.

### 2.1.1 Dynamic etching test

In this test, core samples are etched with acid system under certain conditions of contact time, pumping rate, temperature, and leakoff differential pressure.

The experimental apparatus used was described by Melendez (2007). Fig. 2 is a schematic of the experimental apparatus:

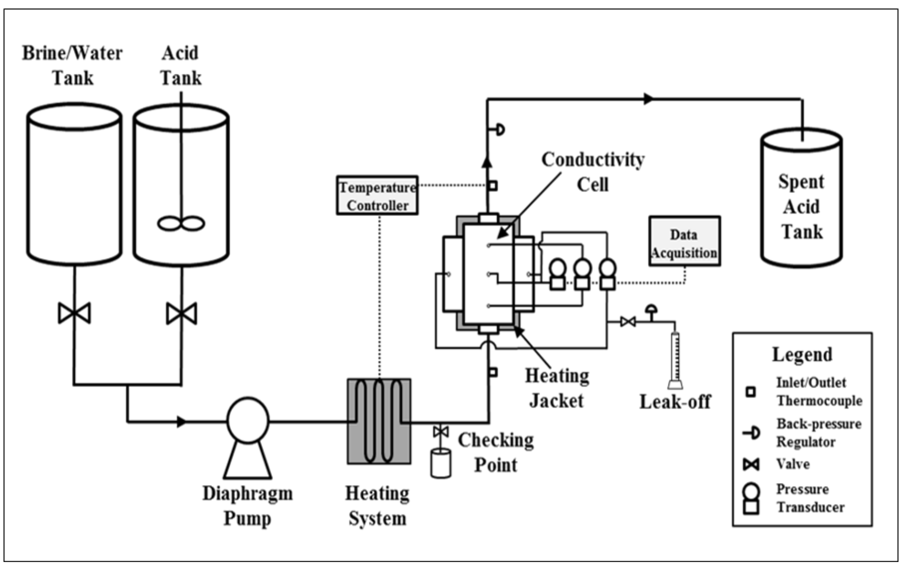


**Figure 2: Schematic of the dynamic etching test experimental apparatus**

A modified API RP-61 conductivity cell was used as a test cell in this work (Fig.3). The cell is made of corrosion-resistant Hastelloy material to prevent acid from damaging the cell.

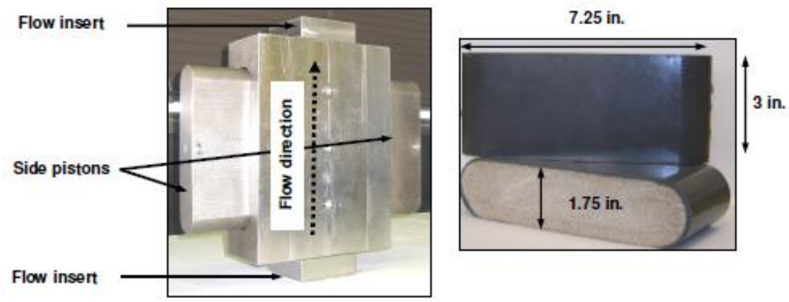


**Figure 3: Modified API RP-61 conductivity cell**

The inside of the cell is designed to accommodate 7-in. long, 1.7-in. wide, 3-in. thick core samples. The core samples are rectangular in shape with rounded edges and have the shape of the inside of the cell to provide a good fit and prevent the leakoff of acid from around the core (outer side of core). The cell has inner O-rings as an extra measure to prevent leakoff of fluids. Pistons equipped with O-rings are used to hold the cores in place and allow for flow of the fluid leaked off through the cores.

The pressure of the cell is set at 1000 psi using a back-pressure regulator to ensure that $CO_2$ (a product of the reaction between carbonate rock and HCl acid) is dissolved in the acid. A leakoff pressure of 20 psi is set using a back-pressure regulator to allow for fluid flow through the core samples. The core samples are placed vertically to eliminate gravity effect, which affects the etching pattern on fracture surfaces. A fracture width of 0.12 in. is achieved by using a shim. Acid and water are injected using a diaphragm pump capable of pumping 1 liter/min. A heating system comprised of heating tape was used to obtain the desired treatment temperature.  Two thermocouples are used to measure the temperature of acid upstream and downstream of test cell to study the temperature behavior due to acid reaction. Pressure transducers are used to measure pressure differential along the fracture, pressure leakoff differential, and cell pressure. All pressure transducers are connected to a computer where pressure data are recorded digitally using labView software. The volume of leaked fluid as function of contact time is measured for each experiment.

### 2.1.2 Surface characterization

A profilometer device (Fig. 4) is used to scan the fracture surfaces before and after each dynamic etching test. This device precisely measures the vertical variation of fracture face topography before and after etching at each sampling point. A laser displacement sensor measures the vertical distance to the fracture face. The vertical measurement resolution of the device is 0.002 in. and the horizontal measurement resolution is 0.05 in. Full details about the device and the labView software are presented by Malagon (2006).

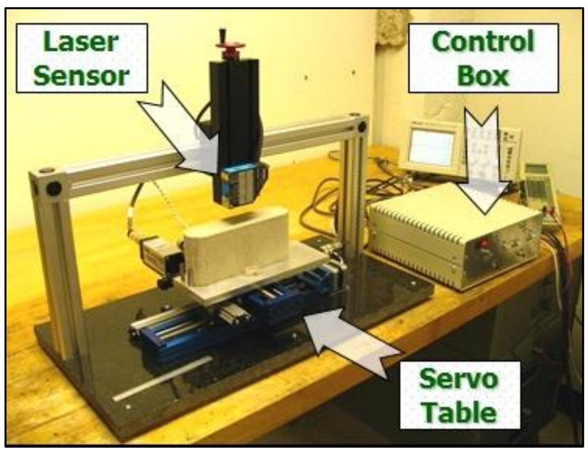


**Figure 4: Profilometer components. (modified from Malagon, 2006)**

Recorded data are processed using in-house developed software, which calculates volume of rock etched and generates a 2-D contour of the core surface topography.

### 2.1.3 Conductivity test

The conductivity of the etched fracture surfaces at increments of closure stress is measured in this test. Fig. 5 shows a schematic of conductivity test apparatus:

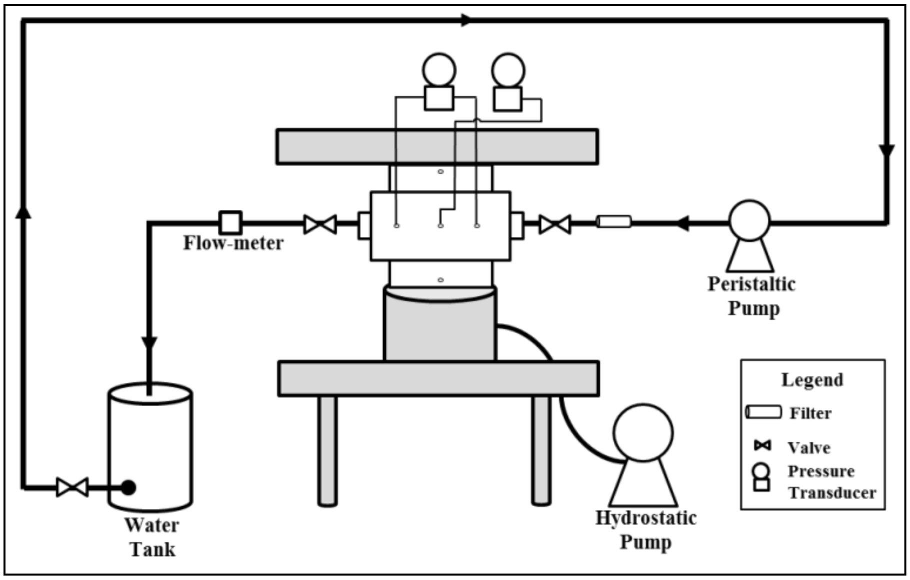


**Figure 5: Schematic of conductivity test experimental apparatus**

The same cell (modified API RP-61) is used in this setup. The cell is placed horizontally inside the load frame, which exerts the required closure stress value. A peristaltic pump is used to inject the testing fluid (tap water) and a flowmeter is used to measure the injection rate. Pressure differential along the fracture and inside the cell are measured using pressure transducers. The flow direction in the conductivity test is opposite to the acid injection direction, representing the production stage of the acid-fracturing treatment.

## 2.2 Equipment Description

### 2.2.1 Diaphragm pump

To inject acid into the test cell at the required rates, a diaphragm pump was used (see Fig. 6). The pump has a pumping maximum rate of 1.4 l/min at a maximum operating pressure of 2,200 psi, and it has a calibration from 0 to 100%. The pump is used to inject water during the pressure test and while the system warms up as well as to inject acid during the dynamic etching test.

**Figure 6: Diaphragm pump capable of pumping 1.4 l/min at max pressure of 2,200 psi**

### 2.2.2 Pressure transducers

To monitor and measure pressure differential along the fracture, leakoff pressure differential, and pressure inside the cell, three transducers with different pressure ratings are used (Fig. 7). The fracture differential, leakoff differential, and cell pressure transducers are rated for 30, 30, and 1,500 psi, respectively.

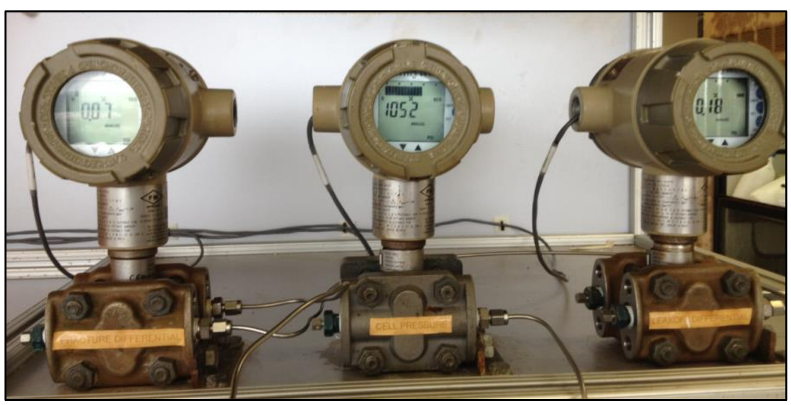


**Figure 7: Pressure transducers used in dynamic etching test experiment**

Similar types of transducers are used in conductivity test setup to measure the pressure difference along the fracture and cell pressure. These pressure devices are connected to a computer where data are recorded and plotted digitally using labView software.

### 2.2.3 Load frame

The conductivity cell is placed horizontally inside the load frame, which is capable of exerting a closure pressure of up to 10,000 psi (Fig. 8). The load frame has a ram area of 125 in.$^2$ and is capable of producing up to 250,000-lbf force. Because the cross-sectional area of the cores is 1/10 to the load-frame ram area, the overburden pressure applied to the cores is 10 times the load-frame pressure.

**Figure 8: Load frame capable of exerting 10,000-psi closure stress**

### 2.2.4 Vacuum pump

The purpose of the vacuum pump is to create vacuum by sucking the air inside of the container to allow for saturating the core with water. A pressure gauge is mounted on the container to monitor the internal pressure and to ensure that cores are fully saturated with water (Fig. 9). The process lasts until a pressure close to zero psi is reached.

**Figure 9: Vacuum pump for saturating cores with tap water**

### 2.2.5 Modified API RP-61 conductivity cell

The conductivity cell consists of the cell body, two flow inserts, and two side pistons, all being made of Hastelloy material (Fig. 10). The cell is 10-in. long, 3-1/4-in. wide, and 8-in. in height to accommodate two core samples with the following dimensions: 7-in. long by 1.7-in. wide by 3-in. in height. There are three access ports in one side of the cell body that are connected to three transducers through the flowlines. The side pistons, equipped with O-rings, have a cross-sectional area of 12.5 in. and have access ports to allow for flow of the fluid that leaks off through the matrix. The two flow inserts, also equipped with O-rings, are connected to the flowlines at the inlet and outlet of the cell body. More details are presented by Pongthunya (2007).

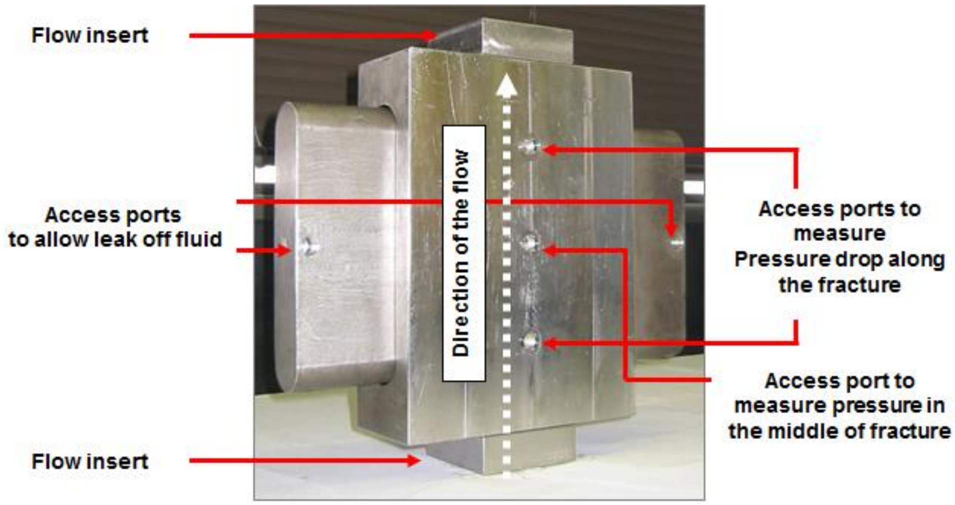


**Figure 10: Description of Modified API RI-61 conductivity cell**

### 2.2.6 Backpressure regulators

Two backpressure regulators are used to achieve a cell pressure of 1,000 psi and a leakoff pressure differential of 20 psi (Fig. 11). A 1,000-psi backpressure is applied to the cell downstream using a nitrogen tank to ensure that $CO_2$, generated as a product of the reaction of HCl acid with dolomite cores, remains dissolved in the spent acid. A 980-psi pressure is applied to the leakoff flow tubes to achieve a 20-psi pressure differential, allowing for the fluid to leak off through the cores during the dynamic etching test.


**Figure 11: Backpressure regulators used in the acid etching setup**

### 2.2.7 Heating system and thermocouples

A heating system is employed to heat the injected fluids to a specific temperature before they enter the cell and react with the fracture surfaces. The system consists of heating tape wrapped around a segment of stainless steel flowline through which fluids pass before entering the test cell (Fig. 12). The heating system is controlled from a control panel where the temperature is set to a specific value and the heating tape operates until the required temperature is achieved. The accuracy of this system is within ± 5 to 10$^{o}$F. Two thermocouples are used to measure the temperature upstream and downstream of the cell.


**Figure 12: Heating tapes, thermocouple, and temperature control panel**

## 2.3 Experimental Procedure and Output

An experimental workflow consisting of five consecutive steps was adopted throughout this study. The sequence of these steps is demonstrated in the following flow chart (Fig.13):

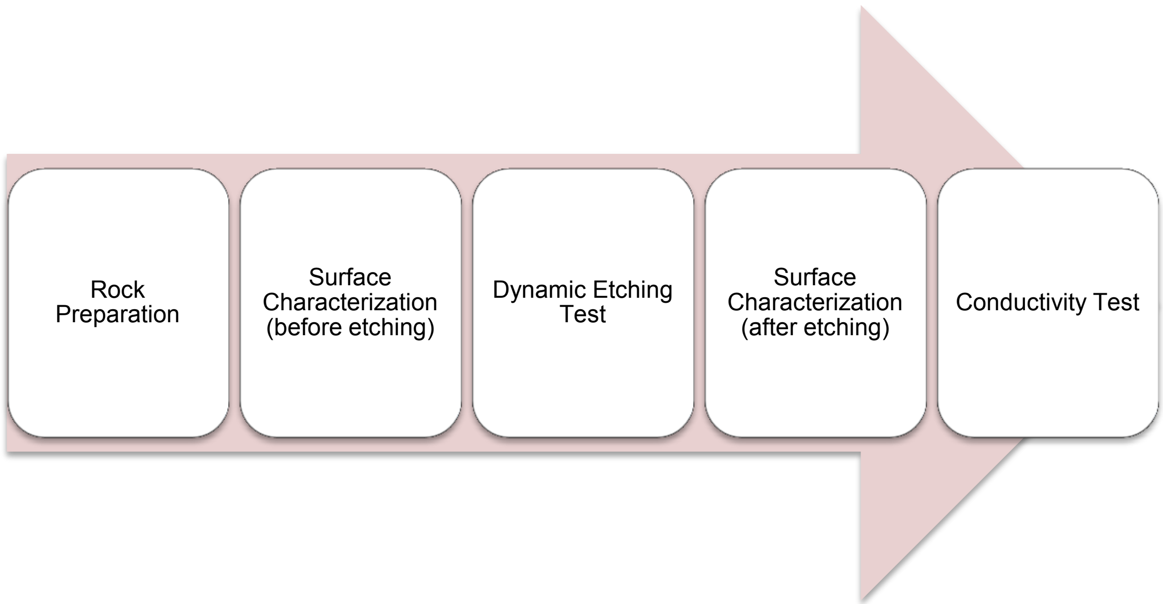


**Figure 13: Flow chart for acid-fracture conductivity study**

### 2.3.1 Rock preparation

The source of core samples can be outcrop or actual reservoir rocks. For this study, cores were cut from San Andres dolomite outcrops. Two sets of initial conditions of fracture surfaces were investigated and each required a special core sample cutting procedure. Initially, the core samples, cut out of the rock, were rectangular with rounded edges and measured 7-in. long, 1.7-in. wide, and 6-in. thick. The differences in creating each surface type are described below.

- **Smooth surface fracture**: Similar to earlier work performed by Melendez (2007) and Pournik (2008), an electric cutter machine is employed to cut each core into halves. Fig.14 shows the top and side views of a smooth surface core sample.

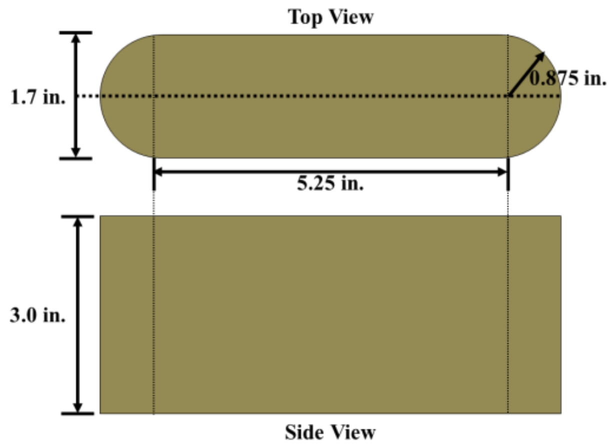


**Figure 14: Smooth-surface core dimensions**

- **Rough surface fracture**: Various techniques are described in the literature to impose a tensile fracture into a rock. The three-point test is an example of these techniques (Fig.15). We chose to simplify the technique by hitting and cracking the core into two equal sections by using a chisel. Fig.16 shows the top and side view of rough surface cores. The procedure is simple and repeatable.

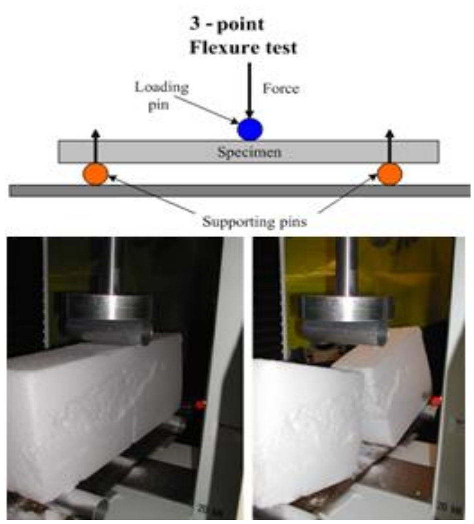


**Figure 15: Three-point test**

**Figure 16: Rough-surface cores**

After cutting the cores, they  were covered with a silicon-based sealant  that provides a perfect fit for cores inside the conductivity cell, which in turn prevents any leak between the outside of cores and the cell body (Fig.17). The complete details of core coating and preparation were presented by Melendez (2007).

**Figure 17: Coated core samples**

### 2.3.2 Surface characterization before and after etching

The core surfaces are scanned before and after each acid-etching test using the profilometer. The first scan serves as a baseline to be compared with cores after being etched with acid. The second scan is aimed at studying the effect of acid on the etching pattern as well as the etched volume of the core surface.

The results of these steps are a 2-D contour of the etching pattern created by acid (Fig.18) and the volume of rock etched. The scale to the right of the 2-D contour represents the difference in vertical distance in inches between the two scans, which is used to calculate the volume of rock etched. 2-D contour and volume calculations are performed using an in-house built Matlab program. Malagon (2006) presented the code for the Matlab program.

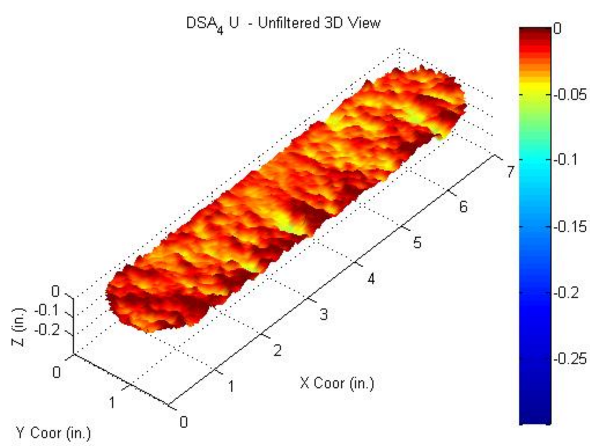


**Figure 18: 2-D contour of a core surface**

### 2.3.3 Dynamic etching test

To perform this test, an acid system is prepared inside the acid tank. Two types of acid systems were examined in this study, linear gelled 15-wt% HCl acid and in-situ crosslinked acid. Table 1 show the formulation used to prepare 12 liters of linear gelled 15-wt % HCl acid.

**Table 1: Formulation to prepare 12 liters of linear gelled 15-wt% HCl acid**

| **Acid Type** | **Linear Gelled** | |
|---|---|---|
| **Volume** | 12 | l |
| **$H_2O$** | 3515.35 | ml |
| **Corrosion Inhibitor** | 36 | ml |
| **Iron Stabilizer** | 14.37 | mg |
| **HCl (36%)** | 4393.3 | ml |
| **$H_2O$** | 3515.35 | ml |
| **Gelling agent** | 540 | ml |

This acid system consists of 0.3-vol% corrosion inhibitor, 4.5-vol% water-soluble polymer, and an iron stabilizer. After adding these components, the acid is mixed using both overhead and magnetic stirrers to generate a well-mixed, homogenous fluid with the designed rheology.

An example of rheology measurement of this linear gelled 15-wt% HCl acid at different shear rates is shown in Table 2:

**Table 2: Rheology measurements of linear gelled 15-wt% HCl acid**

| **Rheology Measurements @75°F** | |
|---|---|
| **RPM** | **Dial Reading** |
| 3 | 12 |
| 6 | 16 |
| 100 | 48 |
| 200 | 67 |
| 300 | 84 |
| 600 | - |

To prepare an in-situ crosslinked acid, the following formulation is adopted (Table 3):

**Table 3: Formulation to prepare 12 liters of in-situ crosslinked 15-wt% HCl acid**

| **Acid Type** | **Crosslinked Acid** | |
|---|---|---|
| **Volume** | 12 | L |
| **$H_2O$** | 6880 | ml |
| **Corrosion Inhibitor** | 36 | ml |
| **HCl (36%)** | 4393.3 | ml |
| **Iron Control Agent** | 120 | ml |
| **Fluid-loss Control** | 30 | ml |
| **Gelling Agent** | 540 | ml |

The in-situ crosslinked acid system consists of 4.5-vol% water soluble polymer, 0.3-vol% corrosion inhibitor, 1-vol% iron control agent, and 0.25-vol% fluid-loss agent. The crosslinking process is triaged by a pH value of 2.0.

During this step, the cell pressure is set at 1,000 psi using a back-pressure regulator to ensure that $CO_2$ is dissolved in the acid. A 20-psi leakoff pressure is attained using a back-pressure regulator to allow for fluid leakoff through the core samples. A positive displacement pump capable of pumping 1 liter/min was used to inject the acid. A heating system consisting of heating tape and temperature control panel is used to obtain and control the desired treatment temperature.

Water is injected through the system and heated until the treatment temperature is obtained. Then the fluid flow is switched to acid tank. Two thermocouples are used to measure the temperature upstream and downstream regions near the cell body to study the effect of acid etching as a function of temperature. An example of a temperature profile for the upstream and downstream regions of the cell during the etching test is shown in Fig. 19.

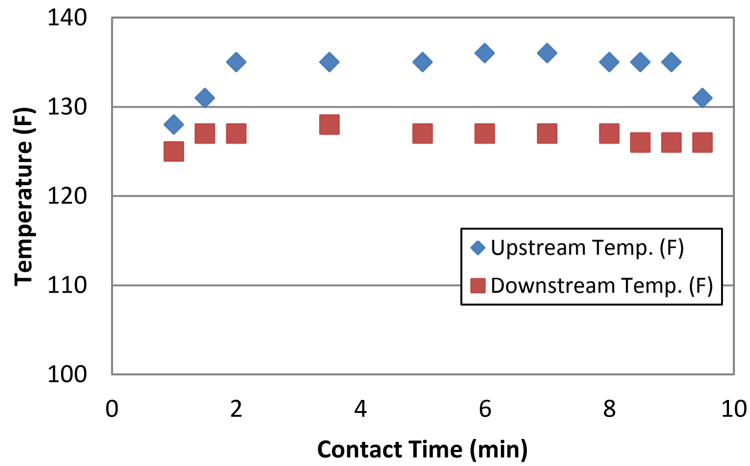


**Figure 19: Upstream and downstream temperature of the cell vs. contact time**

The volume of the leakoff acid is measured in each dynamic etching experiment to study the effectiveness the tested acid system has in controlling acid leakoff through core matrix. The leakoff volume through cores as a function of contact time is shown in Fig. 20:

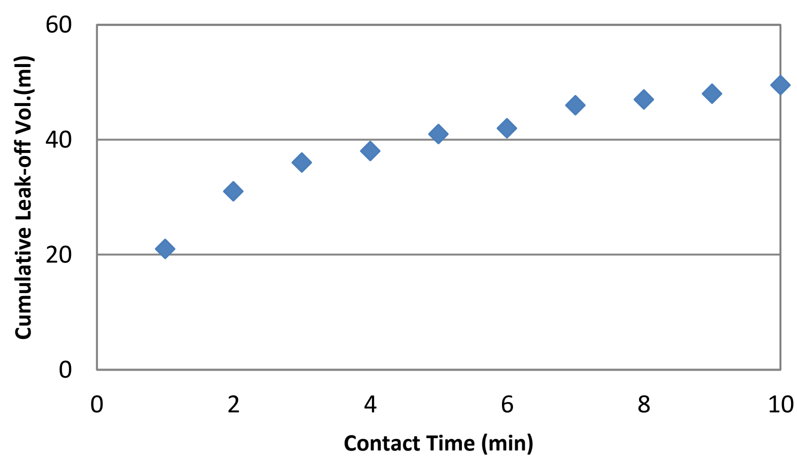


**Figure 20: Cumulative acid leakoff volume vs. contact time**

### 2.3.4 Conductivity measurements

The last step in experiments is to run conductivity tests on etched cores. The test cell is loaded with etched cores and placed horizontally inside of a load frame to provide the required closure stress. Tap water was used as a testing fluid. To calculate fracture conductivity, the pressure drop (ΔP) along the fracture in addition to injection rate (Q) are measured and used in Darcy's equation:

$$wk_f = \mu(\frac{Q}{h})(\frac{L}{\Delta P})$$

where $\mu$ is the testing fluid viscosity, $L$ is the fracture length, and $h$ is the fracture height.

These measurements are made after the injection rate has stabilized and the fracture differential pressure is reached at each closure stress level. The stabilization period varies from one closure stress to another and generally, it takes longer to stabilize at low-closure stress values. Conductivity is measured at a 1,000-psi closure stress increments.

An example of conductivity measurements is shown by Fig. 21.

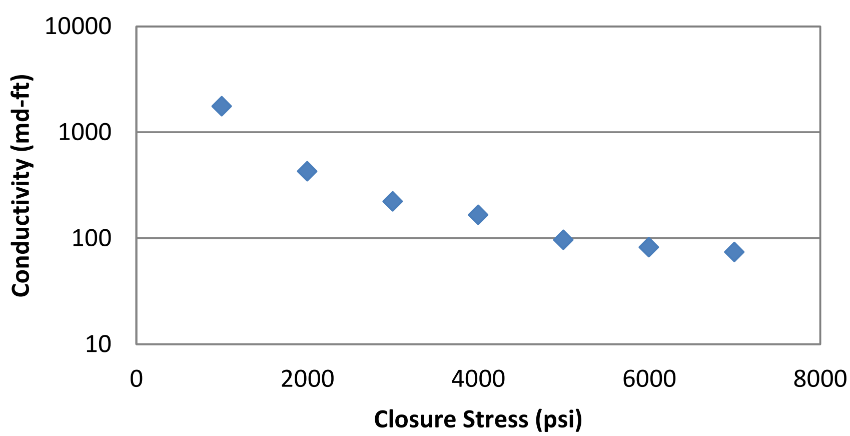


**Figure 21: Conductivity measurements vs. closure stress**

## 2.4 Experimental Variables and Study Plan

The scaled-down experimental conditions described by Pournik (2008) are adopted in this study.

The effects of initial fracture conditions, acid spending, acid system types, treatment temperature and contact time on etched volume, etching pattern, and conductivity of San Andres dolomite was the focus of this study.

The effect resulting from the initial condition of the fracture surface was investigated by running experiments on each fracture surface type under two conditions of contact time and injection rate. The conditions of injection rate and contact time are 0.5 l/min for 20 min and 1.0 l/min for 10 min. This same set of experimental conditions was used to study the effects of the contact time.

A rough surface fracture was used throughout the remaining experiments because it was found to predict the conductivity significantly different compared with a smooth surface fracture and resembles the actual surfaces of a fracture more accurately than smooth surface fracture.

The effect of acid spending as it travels along a fracture was studied by running three experiments at different stages of acid spending. These conditions represent different locations along a fracture when it reacts with acid at different stages of spending, including:

- Fracture entrance reacting with a live acid
- Location along a fracture reacting with half-spent acid
- Location along a fracture reacting with 90% spent acid

The half-spent and 90% spent acids were carefully prepared as a function of the acid concentration as well as the amount of salts ($MgCl_2$ and $CaCl_2$ ions) present in the acid solution when both conditions are reached due to the reaction of linear gelled 15-wt% HCl acid with dolomite formation. Detailed calculations of the amount of ions used to prepare the half- and 90% spent acid are given in the appendix.

The effect resulting from the acid system type was then investigated using both linear-gelled and crosslinked acid. These acid systems were injected at 1.0 l/min for a contact time of 10 min and at two treatment temperatures of 100 and 130°F. The same set of experiments was used to investigate the effect of temperature.

The plan for this study consisted of running a total of 16 experiments that are summarized in Table 4. The experiments were repeated to verify the reproducibility of these experiments.

**Table 4: Study plan matrix**

| Variable | Initial Surface Condition | Acid system | Contact Time (min) | Injection Rate (l/min) | Temp. (F) | Count |
|---|---|---|---|---|---|---|
| **Initial Surface Condition and Contact Time** | rough | linear gelled | 10 | 1 | 130 | 6 |
| | smooth | | | | | |
| | rough | | 20 | 0.5 | | |
| | smooth | | | | | |
| **Acid Spending** | rough | Live linear | 10 | 1 | 130 | 4 |
| | | half spent linear | | | | |
| | | 90% spent linear | | | | |
| **Temperature and Acid System** | rough | linear gelled | 10 | 1 | 100 | 6 |
| | | | | | 130 | |
| | | crosslinked | | | 100 | |
| | | | | | 130 | |

# 3 RESULTS AND DISCUSSION

In this section, the results of a total of 16 experiments on San Andres dolomite cores are discussed. Complete results of these experiments are presented in the appendix. The experiments were grouped into three study plans. Each study plan was aimed to investigate the effect of a certain variable on the rock etched volume, the etching pattern created by acid and the conductivity of etched cores. Variables investigated are the initial condition of fracture surface, the degree of acid spending, the treatment temperature, the acid system types and the contact time. The results of the three study plans and a comparison of the experimental results with the N-K and Deng-Mou correlations are discussed in this section.

## 3.1 Effect of the Initial Condition of the Fracture Surfaces

The effect resulting from the initial condition of the fracture surface on rock etched volume, acid etching pattern and conductivity was investigated by running experiments on each fracture surface type under two conditions of contact time and injection rate.

Smooth- and rough-surface fractures were etched with linear gelled 15-wt% HCl acid at a treatment temperature of 130°F. Table 5 presents the study plan of this investigation.

**Table 5: Study plan for the investigation of the effect of the initial condition of fracture surfaces**

| Variable | Initial Surface Condition | Acid system | Contact Time (min) | Injection Rate (l/min) | Temp. (F) |
|---|---|---|---|---|---|
| **Initial Surface Condition and Contact Time** | rough | linear gelled | 10 | 1 | 130 |
| | smooth | | | | |
| | rough | | 20 | 0.5 | |
| | smooth | | | | |

Etched volumes from surface characterization of smooth- and rough-surface fractures etched at the two conditions of injection rate and contact time are shown in Table 6. A comparison between the rock etched volume with linear-gelled acid of this study with previous results by Melendez (2007) is shown in the appendix.

**Table 6: Etched volume of smooth and rough surface fractures at 10- and 20-min contact times**

| **Sample** | **Contact Time** | **Etched Volume** |
|---|---|---|
| **no.** | **Min** | **$in^3$** |
| DSA-2 (Smooth) | 20 | 0.31 |
| DSA-3 (smooth) | 10 | 0.143 |
| DSA-4 (Rough) | 20 | 0.226 |
| DSA-5 (Rough) | 10 | 0.155 |

Comparing the surface characterization results of different fracture surface conditions at the same treatment conditions of 1.0 l/min for 10 min (Table 6), we observed that the volume of rock etched on a rough-surface fracture was larger than on smooth-surface fractures. This result is possibly because the reaction rate is a function of the rock surface area in contact with the acid; i.e., an increase in surface area results in a more solid exposed surface to the acid (Mumallah 1991).

Figure 22 shows the surface characterization results for a smooth-surface fracture after etching at the two conditions of contact time.

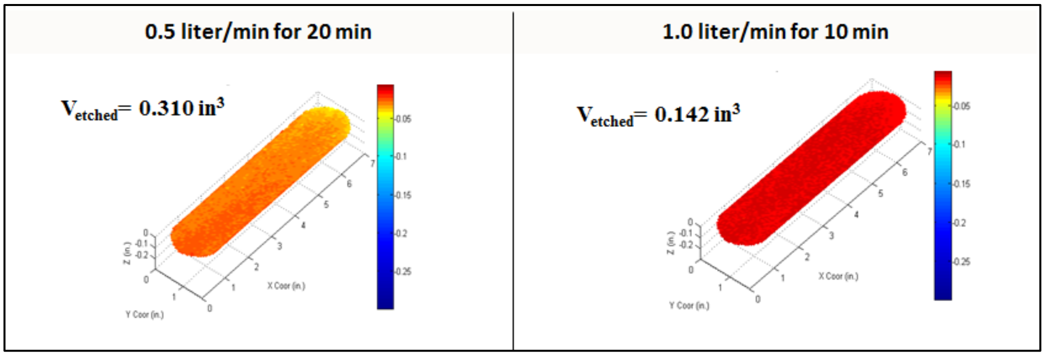


**Figure 22: Etching pattern on a smooth-surface fracture at 10- and 20-min contact times**

A uniform etching pattern was observed under both conditions. These results suggest that the acid creates conductivity on the smooth-surface fracture by surface differential etching, which creates asperities acting like pillars to keep the fracture open at high-closure stress levels.

Comparing the surface topography of both fracture types before and after acid etching showed that acid etched the rough-surface fracture (Fig. 23) in a different pattern compared with a smooth-surface fracture (Fig. 22).

Fig. 24 shows a plot of the vertical distance measurements from the laser sensor of the profilometer to the core surface (z) vs. the difference in vertical distance from the fracture surface before and after acid etching (Δz). The smaller values of z correspond to high points (peaks) while the larger z values correspond to low points (valleys) on the rough-surfaces fracture.  Also, the larger the Δz is, the more the smoothing or the etching effect.

The results of Fig. 24 suggest that acid preferentially etched the high points on the rough-surface more than the low points. This is possibly because it takes a shorter distance for acid to diffuse to the high points compared with low points.  This type of etching pattern enhances the conductivity by widening the distance between fracture-surfaces after closure.

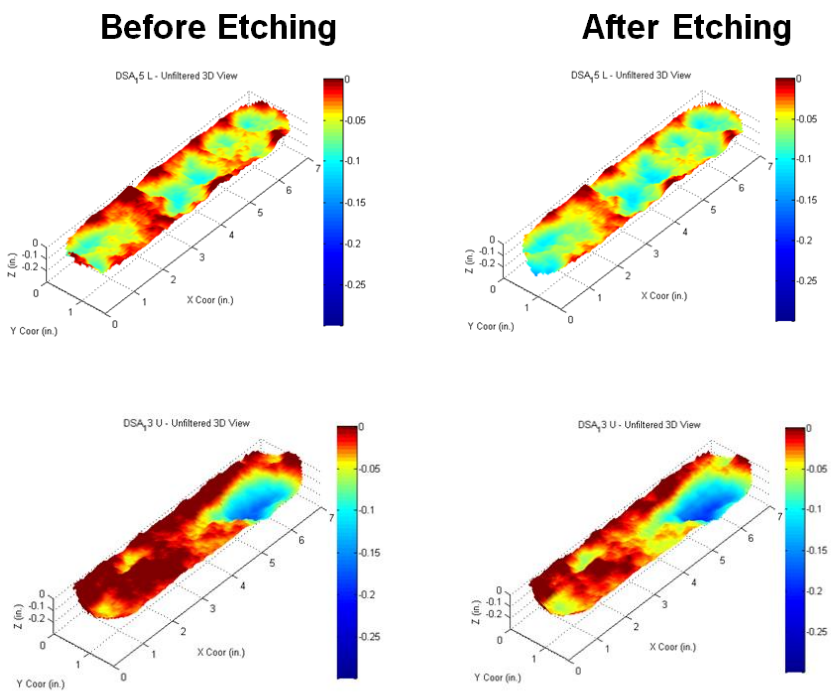


**Figure 23: Etching pattern on a rough-surface fracture**

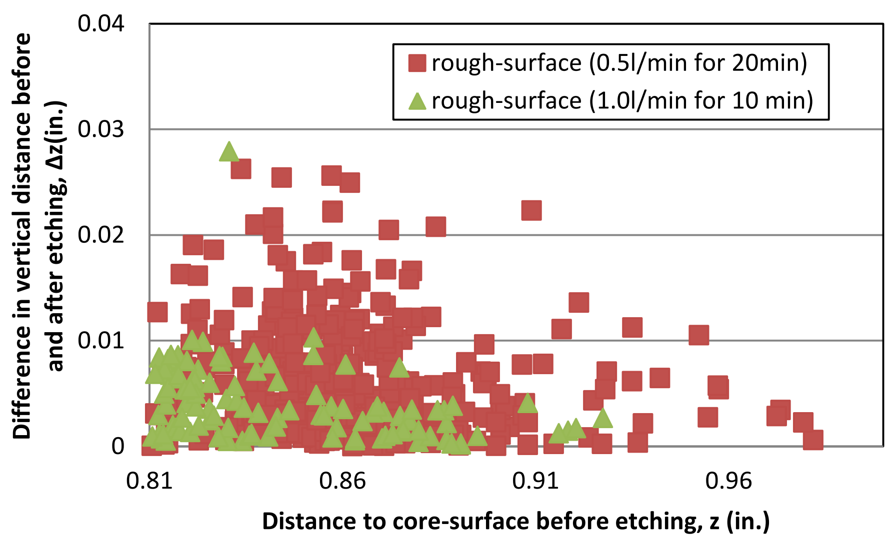


**Figure 24: Etching pattern on a rough-surface fracture at 10- and 20-min contact time**

Figure 25 shows conductivity measurements of both smooth- and rough-surface fractures etched at the shorter contact time.

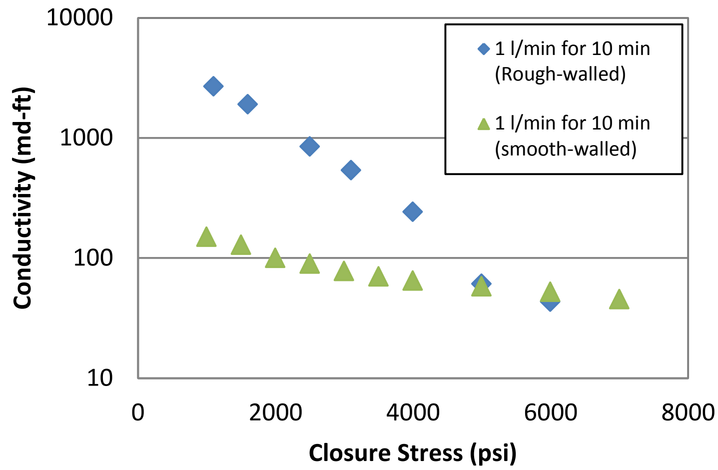


**Figure 25: Conductivity as a function of closure stress for rough- vs. smooth-surface cores etched at 1.0 l/min for 10 min**

The rough-surface fracture showed higher conductivity compared with the smooth-surface fracture. The conductivity difference is one order of magnitude at low-closure stress levels. As the closure stress increased beyond 4,000 psi, the conductivity for both fracture surfaces converges to the same value. This result is possibly because at high-closure stress, the majority of the contact area holding the rough-surface fracture open is crushed, which causes both fracture surface types to behave in the same way.

Conductivity measurements for both fracture types etched at the longer contact times are shown in Fig. 26. Similarly, the rough-surface fracture showed higher conductivity and the difference between the two fracture types is an order of magnitude at low-closure stress

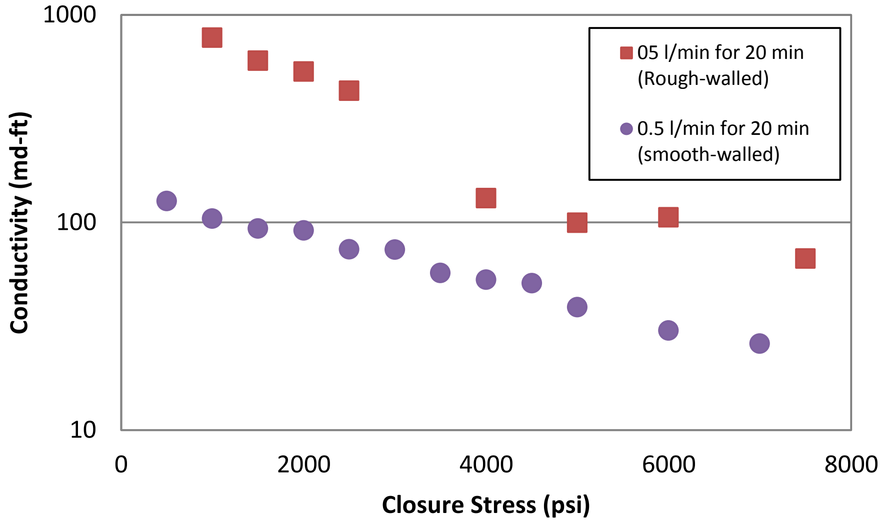


**Figure 26: Conductivity as a function of closure stress for rough vs. smooth surface cores etched at 0.5 l/min for 20 min**

Conductivity measurements for the four experiments are shown in Fig. 27. We can conclude that conductivity created by a rough-surface fracture is greater than conductivity created by a smooth-surface fracture under the two conditions of contact time. This result is likely because a rough-surface fracture has more contact points compared with a smooth-surface fracture, which results in higher conductivity at low closure stress.

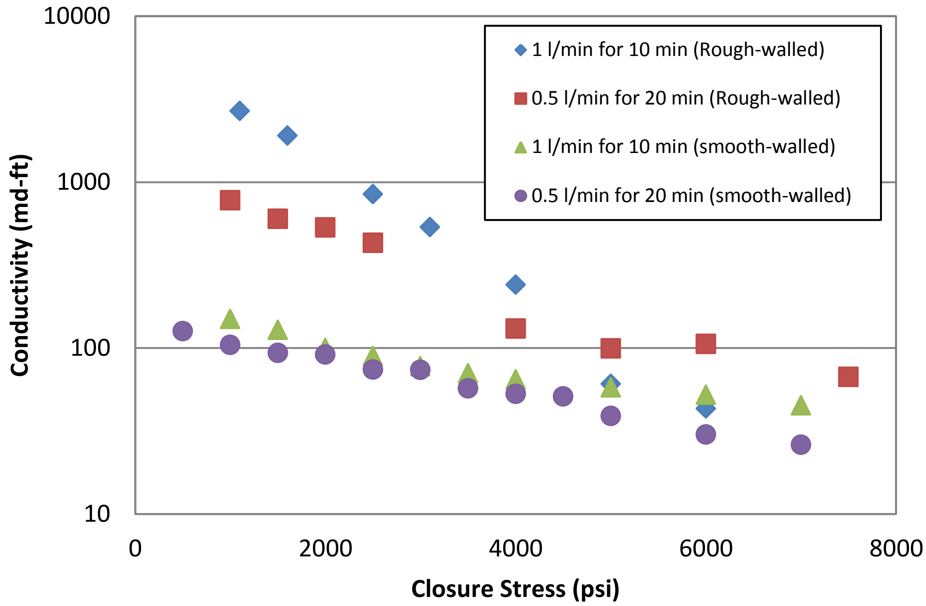


**Figure 27: Conductivity as a function of closure stress for rough- vs. smooth-surface cores etched at 1.0 l/min for 10 and 0.5 l/min for 20 min**

The repeatability of the experiments was confirmed by conducting an experiment for the longer contact time condition. Fig. 28 shows the conductivity results of the two experiments in which both experiments generated approximately the same conductivity profile.

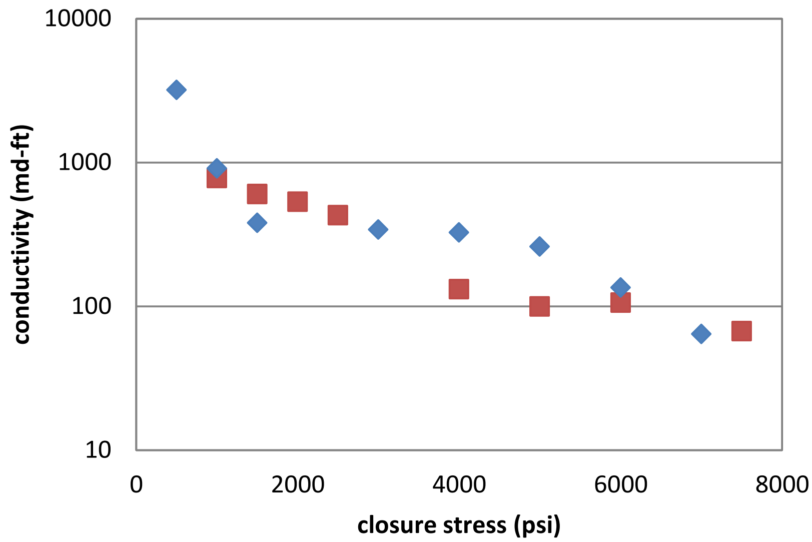


**Figure 28: Repeatability of experiments on rough surface cores etched at 0.5 l/min for 20 min**

## 3.2 Effect of Acid Spending

The effect of acid spending as acid travels along a fracture on rock etched volume, acid etching pattern and conductivity of etched cores was studied in this part.

Three experiments were conducted at a treatment temperature of 130°F and an injection rate of 1.0 l/min for 10 minutes on rough-surface fractures while varying the degree of spending of linear-gelled acid. The three conditions of acid are live, half spent, and 90% spent. The study plan is summarized in Table 8.

**Table 7: Study plan for the investigation of the effect of acid spending**

| Variable | Initial Surface Condition | Acid system | Contact Time (min) | Injection Rate (l/min) | Temp. (F) |
|---|---|---|---|---|---|
| **Acid Spending** | rough | Live linear<br>half spent linear<br>90% spent linear | 10 | 1 | 130 |

Surface characterization results of fractures etched at the three conditions of acid spending showed that the relationship between etched volume and acid spending is linear (Fig. 29). This suggests that the presence of $MgCl_2$ and $CaCl_2$ ions in the half spent and 90% spent acid did not retard the reaction rate of HCl with the dolomite core samples.

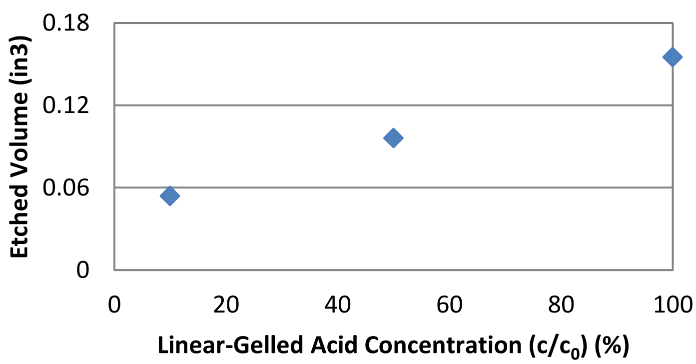


**Figure 29: Etched volume as a function of acid spending**

Figure 30 shows 2-D contour and Fig. 31 shows z vs. Δz plot of rough-surface cores etched at the three acid spending conditions. The surface characterization results showed, 90% spent acid etched the high and low points on the rough-surface almost equally while the live acid etched more of the high points (peaks) compared with the low points (valleys). The results also showed that the higher the concentration of acid, the greater the smoothing of the high points compared with the low points on the rough-surface fractures.

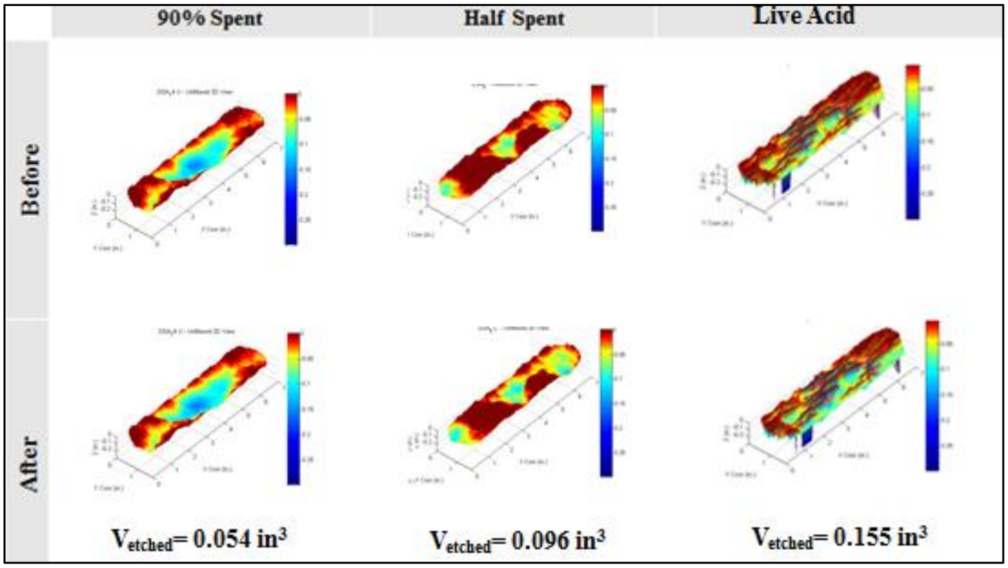


**Figure 30: 2-D contour for cores etched at different stage of acid spending before and after etching**

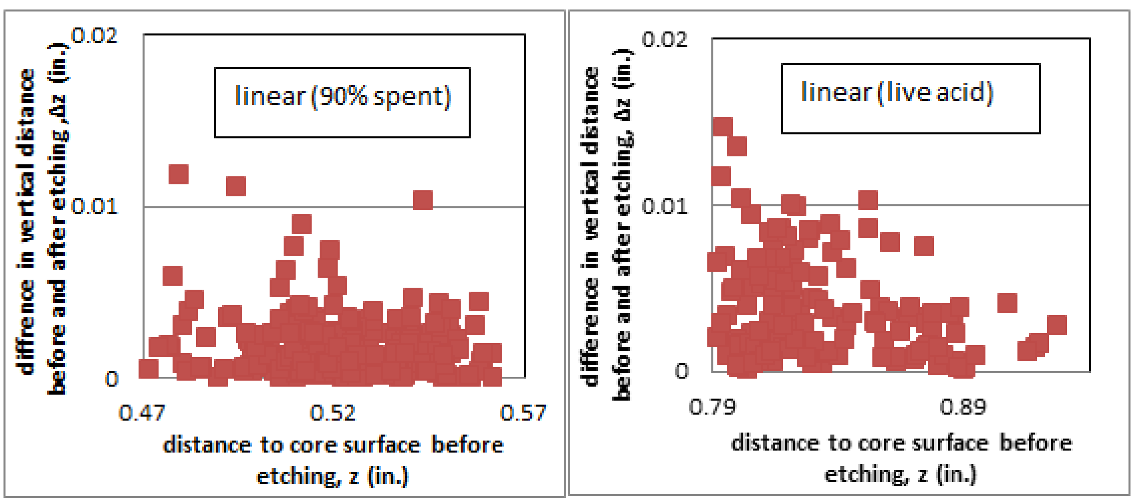


**Figure 31: Etching Patterns for cores etched with 90% spent and live linear-gelled acid**

Conductivity test results for fractures etched under the three acid-spending conditions are shown in Fig. 32. The results indicate that acid spending affects both the etched volume and fracture conductivity.

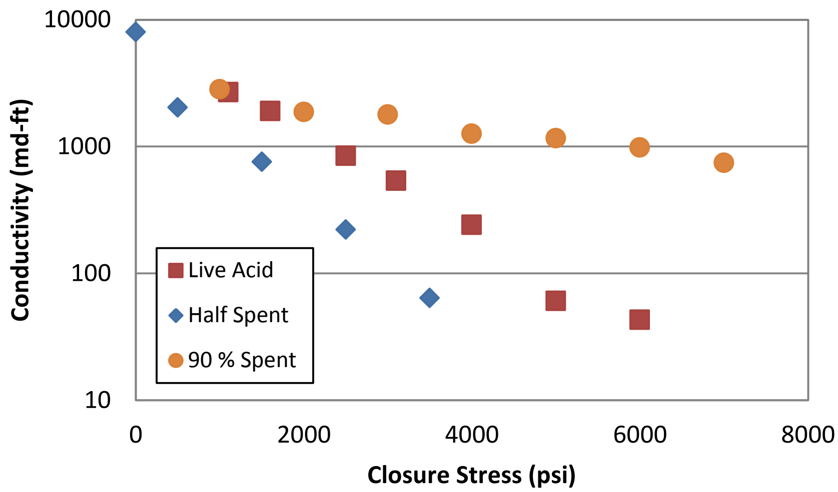


**Figure 32: Effect of acid spending on conductivity**

The conductivity results suggest that an increase in spending does not automatically mean lower conductivity (Fig. 32). This conclusion contradicts previous studies in the literature that always assume lower conductivity with an increase in acid spending. Fig. 33 shows conductivity vs. distance from wellbore plots modified from de Rozieres (1994) and Novotny (1977). Their results suggest that the conductivity of an acid fracture always decreases as the distance from the wellbore increases because of the acid spending effect.

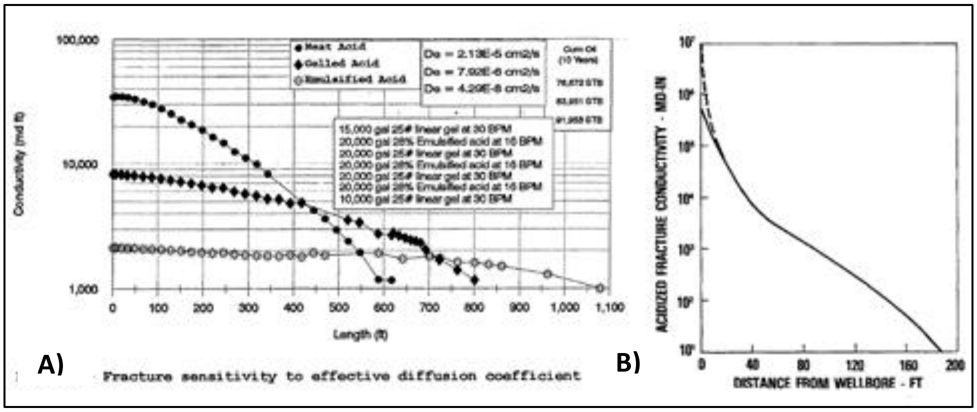


**Figure 33: Conductivity profile as a function of fracture length. A) Modified from de Rozieres (1994). B) Modified from Novotny (1977)**

All three experiments began with the same conductivity value but the fracture-loss conductivity varied with the increase in closure stress. For cores etched with 90% spent acid, the rate of conductivity loss was less than both cores etched with live and 50% spent acid. This result is possibly attributed to reduction of rock compressive strength due to acid etching, which was the least in the case of 90% spent acid. Fig. 34 shows the condition of two cores, one etched with 90% spent and the other with live acid after they were exposed to 7,000-psi closure stress. The cores treated with live acid experienced massive destruction while the cores treated with 90% spent acid were only slightly affected.

Based on these results, etched volume alone is not adequate to predict conductivity. Conductivity is the result of a combination of etching pattern, etched volume, and rock compressive strength after etching.

**Figure 34: Condition of cores after conductivity test: cores etched with 90% spent (left) acid compared to cores etched with live acid (right)**

## 3.3 Effect of Treatment Parameters

### 3.3.1 Temperature effect

The effect of treatment temperature on rock etched volume, etching pattern and conductivity of etched cores were investigated in this part.

Experiments were conducted at two treatment temperatures of 100 and 130°F while injecting the acid systems at 1.0 liter/min for a 10-min contact time. The study plan is shown in Table 9.

**Table 8: Study plan for the investigation of the effect treatment temperature and acid system types**

<table>
<tr><th>Variable</th><th>Initial Surface Condition</th><th>Acid system</th><th>Contact Time (min)</th><th>Injection Rate (l/min)</th><th>Temp. (F)</th></tr>
<tr><td rowspan="4">Temperature and Acid System</td><td rowspan="4">rough</td><td rowspan="2">linear gelled</td><td rowspan="4">10</td><td rowspan="4">1</td><td>100</td></tr>
<tr><td>130</td></tr>
<tr><td rowspan="2">crosslinked</td><td>100</td></tr>
<tr><td>130</td></tr>
</table>

Etched volumes from surface characterization results of all conditions are shown in Fig. 35.

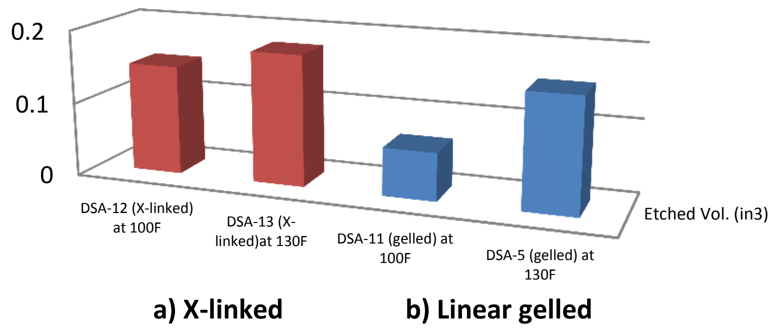


**Figure 35: Etched volume by: a) X-linked acid and b) linear-gelled acid at 100 and 130°F**

The results showed that the higher the temperature, the more the etching for both cores etched with linear and crosslinked acid. However, the difference is more pronounced in the case of linear-gelled acid.

Fig. 36 shows 2-D contour and Fig. 37 shows z vs. Δz plot of two cores before and after they were etched with crosslinked acid at two temperatures. These results showed that the acid smoothed the peaks and deepened the valleys on the rough-surface fractures equally. The results suggest that the etching pattern created by crosslinked acid at different temperatures was the same.

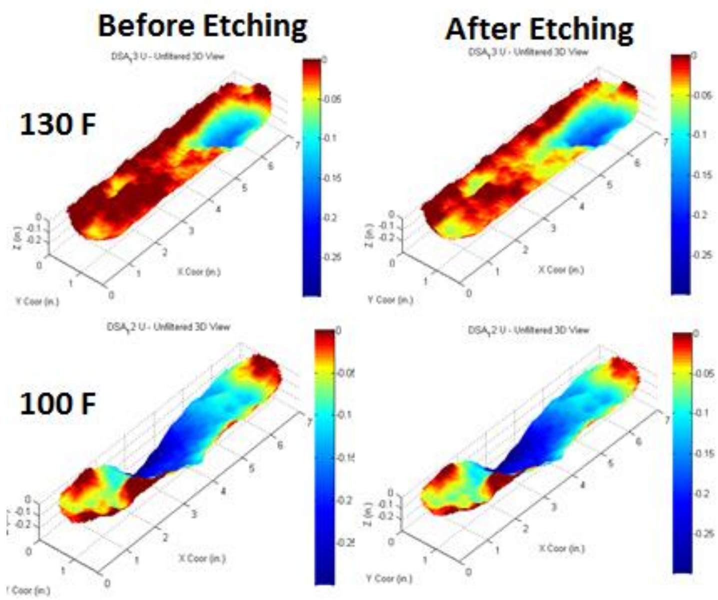


Figure 36: Effect of temperature on etcing pattern for cores etched with crosslinked acid

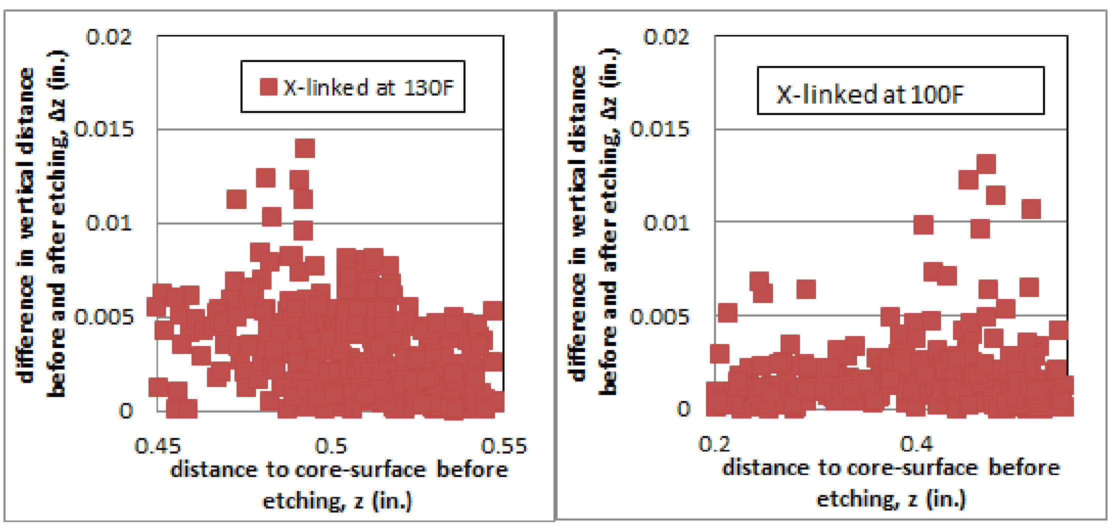


Figure 37: Etching pattern for cores etched with crosslinked acid at 100 and 130$^{o}$F

The results of the conductivity tests showed that cores etched with crosslinked acid at 100°F and 130°F demonstrated a small difference in conductivity (Fig. 38). This small difference correlates with the similarity in etching patterns by acid at the two temperatures (Fig. 37).

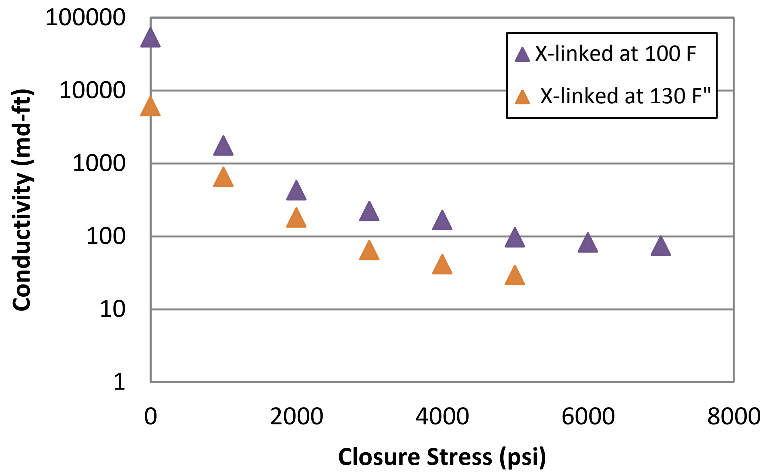


**Figure 38: Effect of temperature on conductivity for cores etched with crosslinked acid**

Fig. 39 shows z vs. Δz plot of two cores before and after they were etched with linear-gelled acid at the two temperatures.

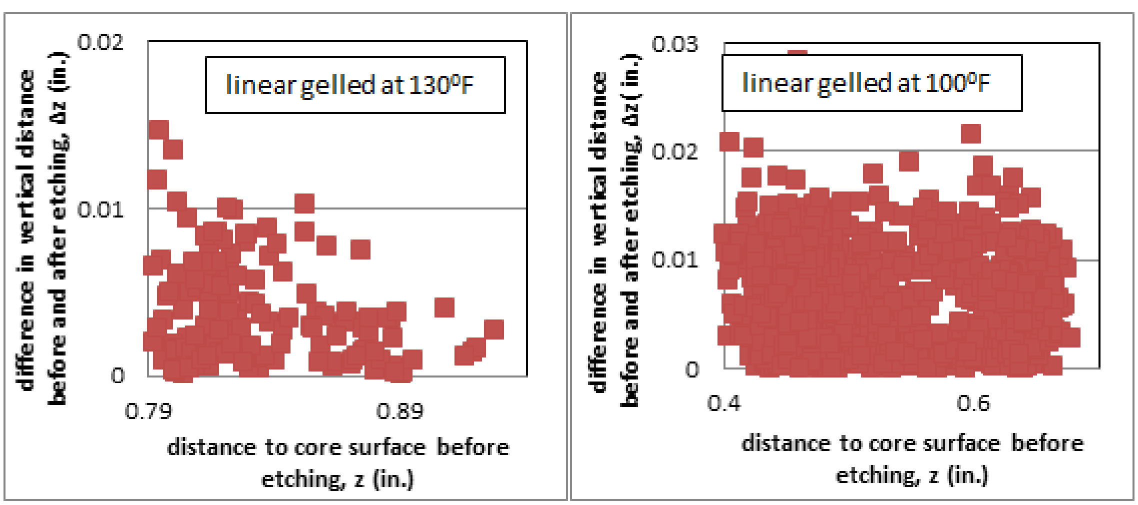


**Figure 39: Etching pattern for cores etched with linear-gelled acid at 100 and 130°F**

The linear-gelled acid at 100°F etched the peaks and valleys equally. However, the acid at 130°F mainly etched the peaks on rough-surface which widens the gap between the fracture-surfaces after fracture closure.

The difference in conductivity between the cores etched with linear-gelled acid at 100°F and 130°F was more pronounced when compared with cores etched with crosslinked acid as shown in Fig. 40. The 130°F treatment created significantly higher conductivity, suggesting that the higher temperature is more preferable when linear-gelled acid is used.

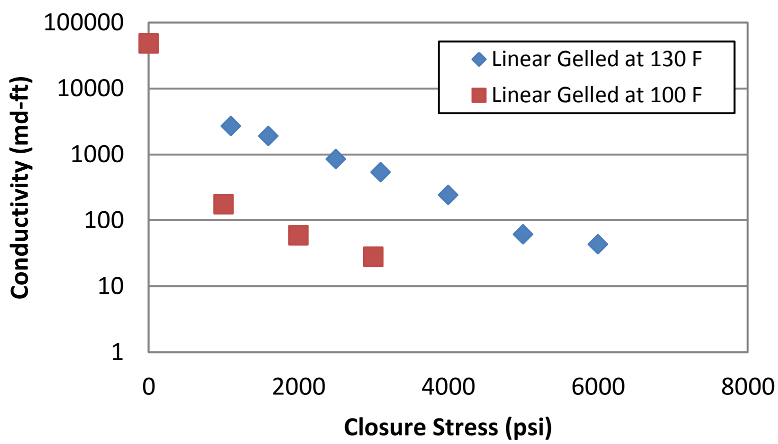


**Figure 40: Temperature effect on conductivity for cores etched with a linear-gelled acid system**

To confirm the repeatability of the results, duplication experiments were conducted for cores etched with linear-gelled acid at 100°F and cores etched with crosslinked acid at 130°F. Fig. 41 shows the conductivity test results for both experiments compared with previous experiments, confirming repeatability.

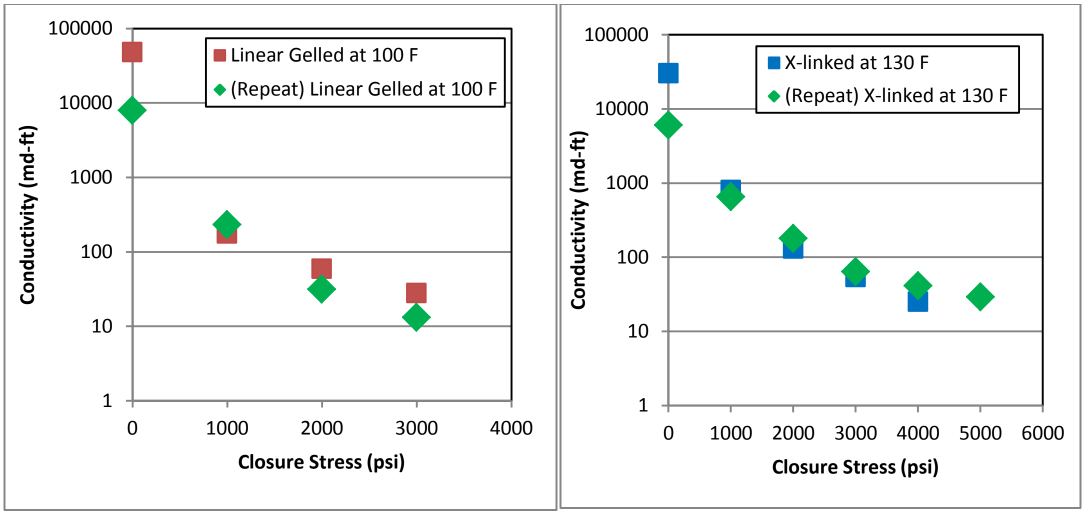


**Figure 41: Repeatability of temperature effect experiments**

### 3.3.2 Acid system type effect

The same set of experiments used to investigate the effect of temperature was used to study the effect of the acid system type on rock etched volume, acid etching pattern and conductivity of etched cores.

One obvious finding from the surface characterization of cores after etching is that crosslinked acid etched more rock volume compared with linear-gelled acid at both treatment temperatures (Fig. 35). This result can possibly be attributed to the effectiveness crosslinked acid has in controlling acid leakoff, which in turn maximizes the etching rate on the fracture surfaces.

The etching patterns were different for each acid type where gelled acid created more and larger pitting compared with crosslinked acid (Fig. 42)

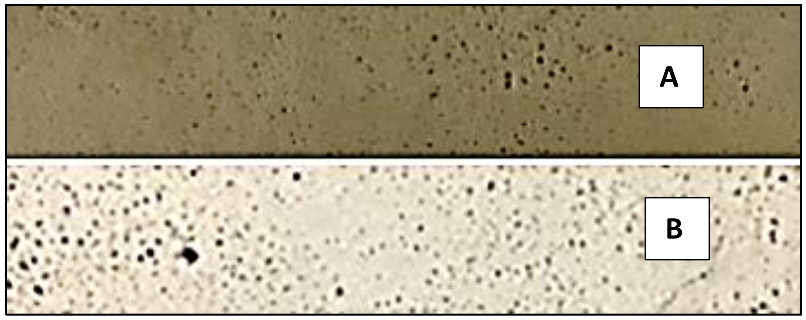


**Figure 42: Closeup pictures of surface of cores etched with: A) linear gelled and B) crosslinked acid**

At a 100°F treatment temperature, rock volume etched by crosslinked acid compared with linear-gelled acid was greater, and the conductivity was higher (Fig. 43).

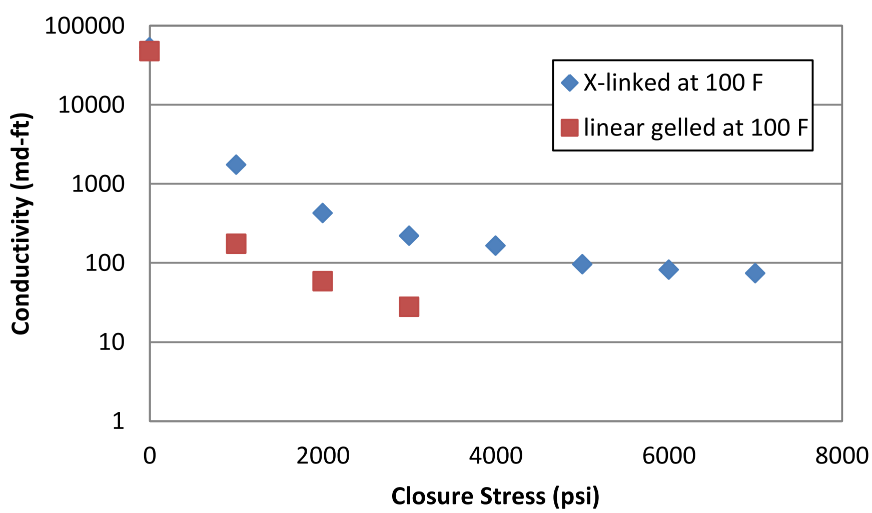


**Figure 43: Effect of acid system type on conductivity at 100°F**

Fig. 44 shows conductivity test results for cores etched with both acid systems at 130°F treatment temperature. Although the volume of rock etched by the crosslinked acid was larger compared with linear-gelled acid, the conductivity generated by the linear-gelled acid was higher. This is possibly attributed to the difference in etching patterns of both acid systems at 130°F.

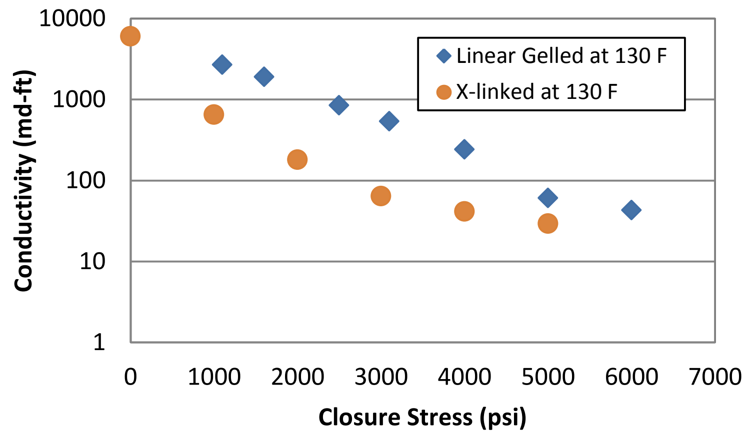


**Figure 44: Effect of acid system type on conductivity at 130°F**

Analyzing the conductivity results of the four experiments (Fig. 46) along with surface characterizations (Fig. 45), and etched volumes (Fig. 35), we observed that conductivity better correlates with etched volume and etching pattern than type of acid system used or treatment temperature.

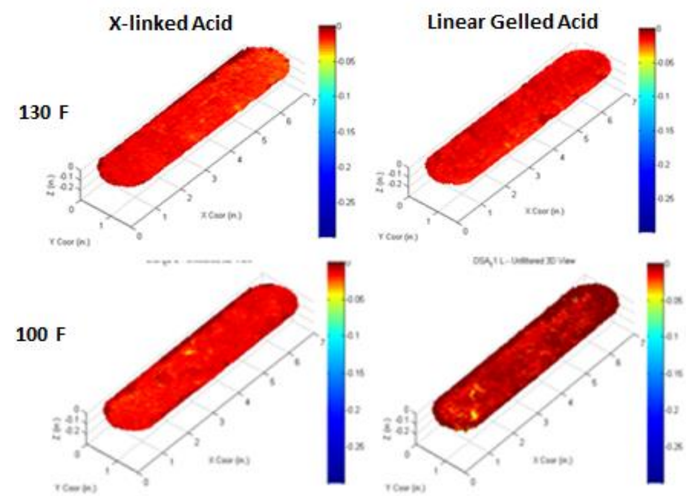


**Figure 45: Difference in etching patterns between linear gelled and crosslinked acid at 100°F and130°F**

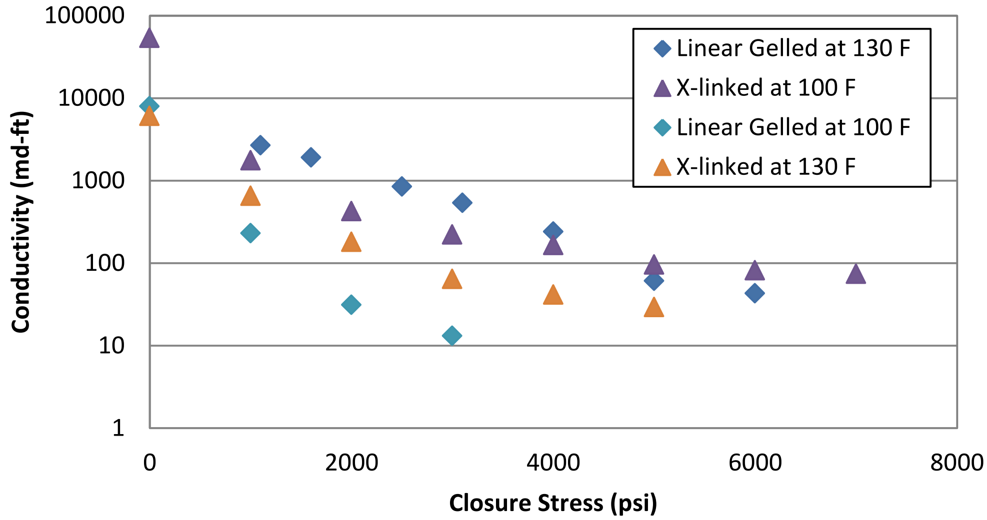


**Figure 46: Effect of acid system type on conductivity**

These results suggest that there is an optimum etched volume and etching pattern in which more or less etching results in a conductivity decrease. This possibly explains why linear-gelled acid created the highest conductivity between the four cases. Linear-gelled acid at 130$^{o}$F, etched large volume of the rock at the optimum etching pattern (etching the peaks more than the valleys) which widens the gap between the fracture-surfaces the most after closure.

To examine the efficiency of linear gelled and crosslinked acid in controlling acid leakoff into the matrix, the volume of leaked acid was measured as a function of contact time during the dynamic etching test (Fig. 8). As shown in Fig. 47, the cumulative volume of acid that leaked into the cores as a function of time behaves as the square root of the time function.  This conclusion suggests that linear-gelled and crosslinked acids are effective as leakoff control at these treatment conditions. The results also showed that crosslinked acid is more effective than linear-gelled acid in controlling acid leakoff.

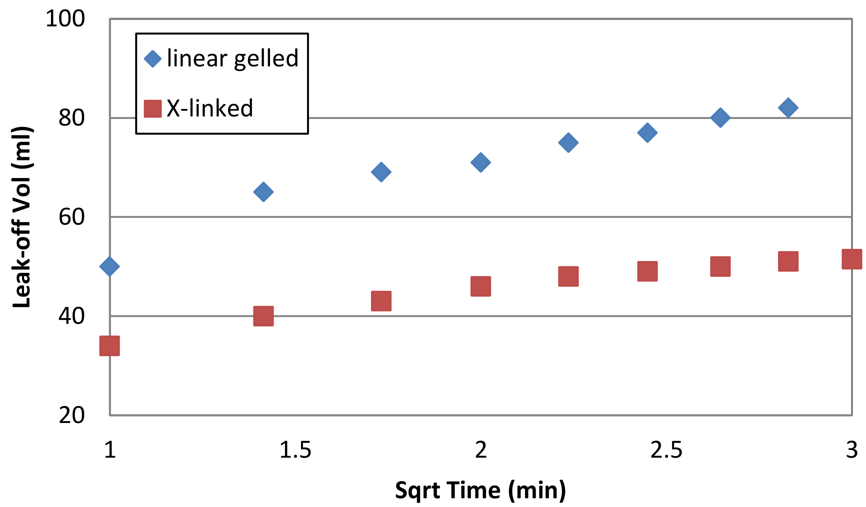


**Figure 47: Cumulative acid leakoff volume as a function of square root of time (Temp=100$^o$F &ΔP=20psi)**

### 3.3.3 Contact time effect

The same experimental plan used to investigate the effect of the initial condition of the fracture surface was used to study the effect of contact time on rock etched volume, acid etching pattern and conductivity of etched cores. Fig. 48 shows the surface scans and etched volume of cores used in this investigation. The volume etched during the longer contact time is twice as much compared with the shorter contact time although the same volume of acid was injected in both conditions. The surface characterization results showed that contact time has no effect on the etching pattern of both smooth- and rough-surface fractures except that the longer contact time smoothed the peaks on rough-surface fracture more than during the shorter contact time (Fig. 49).

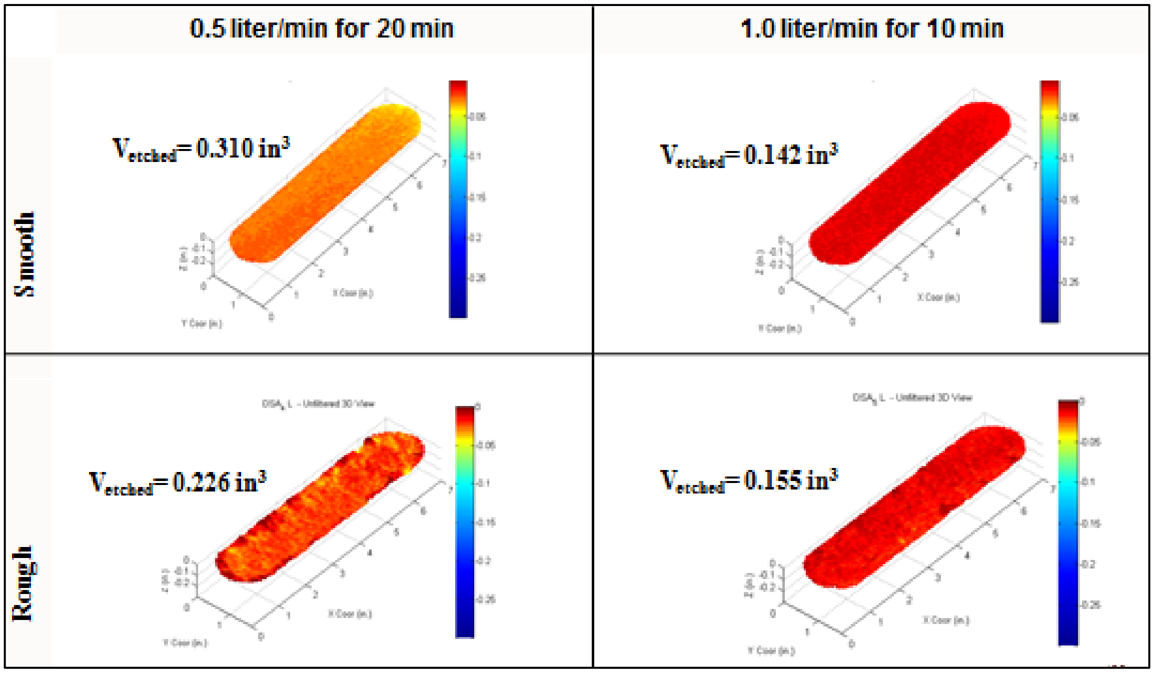


**Figure 48: Effect of contact time on etched volume and etcheing pattern**

Conductivity test results for the four experiments are shown in Fig. 50. For the rough-surface fracture, a shorter contact time created high conductivity compared with a longer contact while injecting the same volume of acid. This result suggests that a shorter contact time is more favorable in this regard, which is likely attributed to the loss of contact points that keep the fracture from closing at longer contact times.

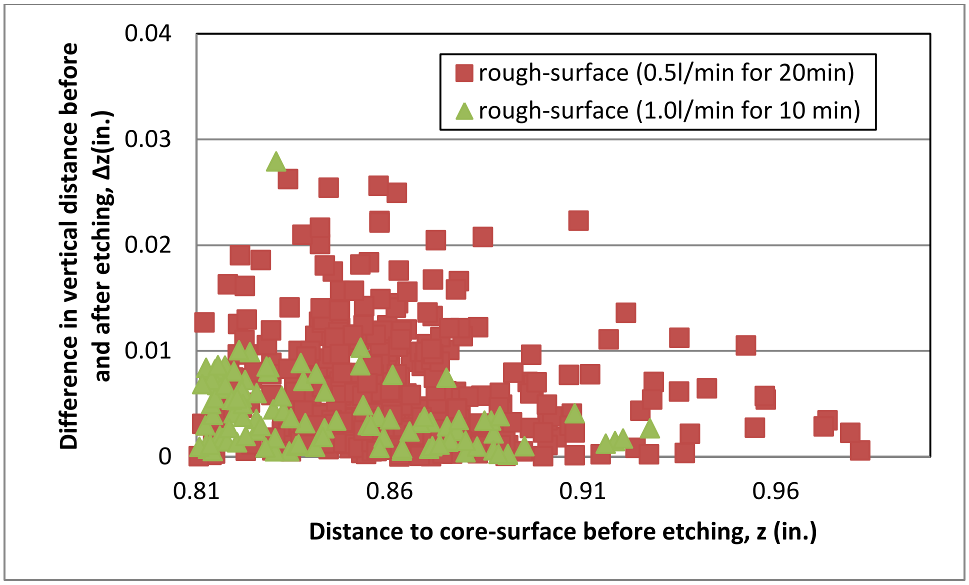


**Figure 49: The difference in etching patterns for rough-surface fractures etched at 10- and 20-min contact time.**

For a smooth-surface fracture, no significant difference in conductivity was observed, which correlates with the same etching patterns generated at both contact times.

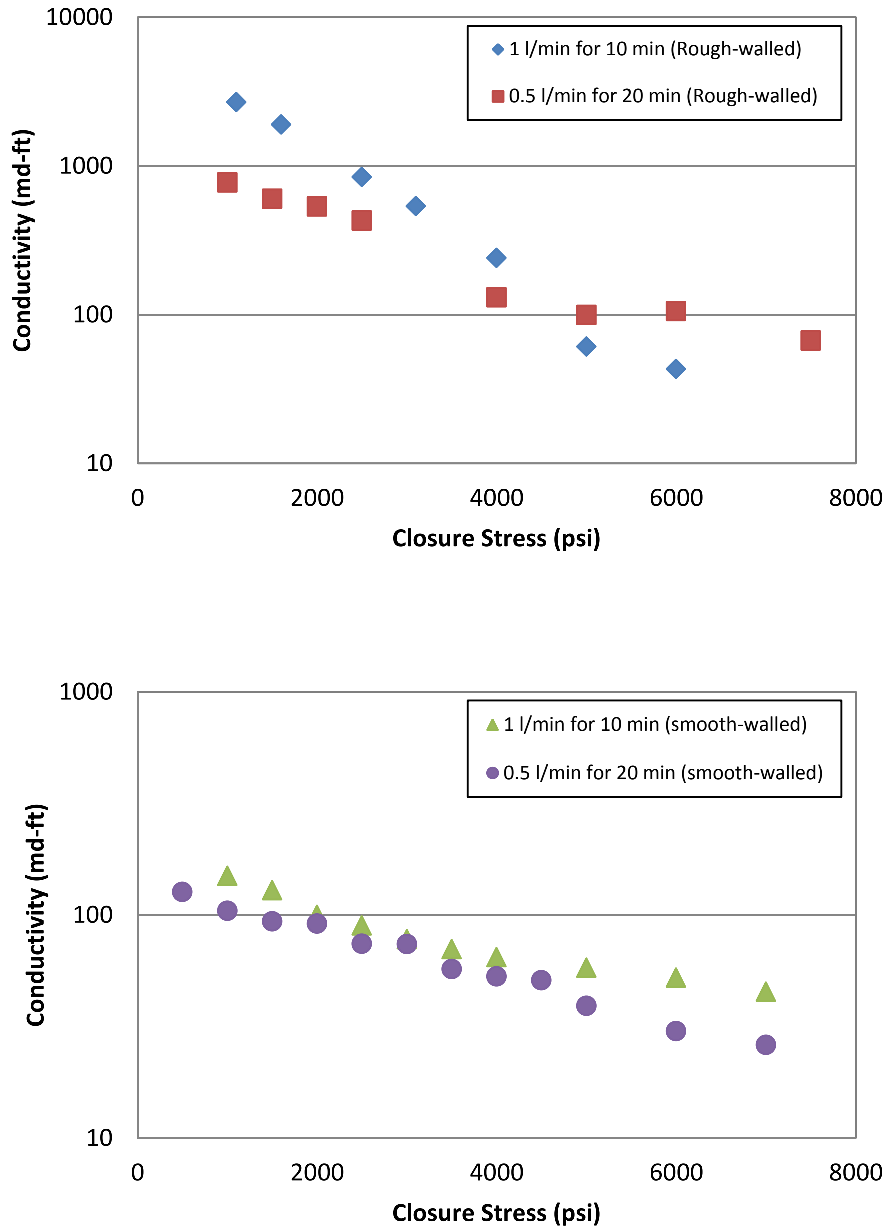


**Figure 50: Effect of contact time on conductivity of smooth- and rough-surface fractures**

### 3.4 Comparison with Correlations

To use the N-K correlation, we need to estimate both $w_i$ and RES. To calculate $w_i$, the volume of rock etched by the acid was estimated using profilometer data and used in the following equation:

$$w_i = \frac{volume\ of\ rock\ etched\ by\ acid}{core\ surface\ area * (1 - \varphi)}$$

For RES, an average value for the San Andres dolomite of 58,080 psi was obtained from previous published data by Melendez (2007) and Pournik (2008).

Deng-Mou correlation for permeability-distribution-dominant case was used because it better represents the acid etching of dolomite compared with other models. Table 9 shows the parameters used by Deng et al. (2012) in their sample calculation.

**Table 9: Paramters for Deng-Mou correlation**

| Parameter | Value |
|---|---|
| $\lambda_{D,X}$ | 0.7 |
| $\lambda_{D,z}$ | 0.0156 |
| $\sigma_D$ | 0.7 |
| E (Mpsi) | 4 |

#### 3.4.1 Smooth-surface fractures

Comparing the experimental results of smooth-surface fractures with the N-K and the Deng-Mou correlations showed that both correlations predictions were inconsistent with the results. The N-K correlation (Fig. 51) overestimated the conductivity compared with one experiment and underestimated the conductivity in the other experiment while the Deng-Mou correlation overestimated the conductivity in both cases.

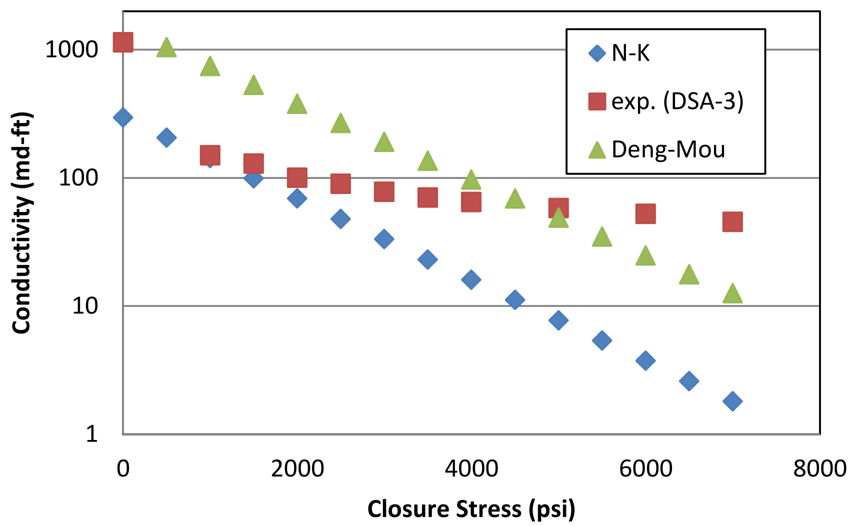


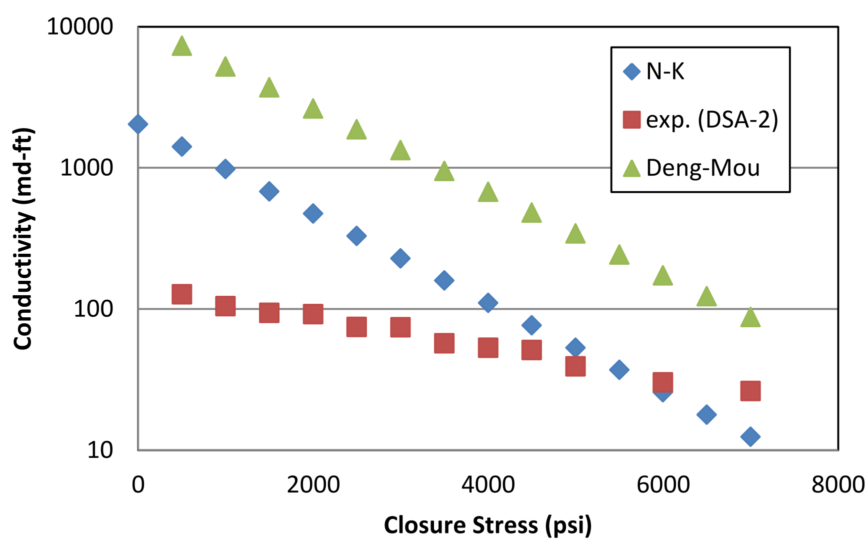


**Figure 51: Comparison between experimental results vs. the N-K and Deng-Mou correlations for conductivity of smooth-surface cores**

### 3.4.2 Rough-surface fractures

Conductivity measurements of rough-surface fractures showed that an increase in etched volume does not always translate into higher conductivity. One of the shortcomings of the N-K correlation is that it always assumes higher conductivity for higher etched volume, given the same rock-embedment strength. For all the experiments conducted on rough-surface fractures, the N-K correlation underestimated the conductivity values (Fig. 52). On the other hand, the Deng-Mou correlation showed a better prediction to experimental results compared with the N-K.

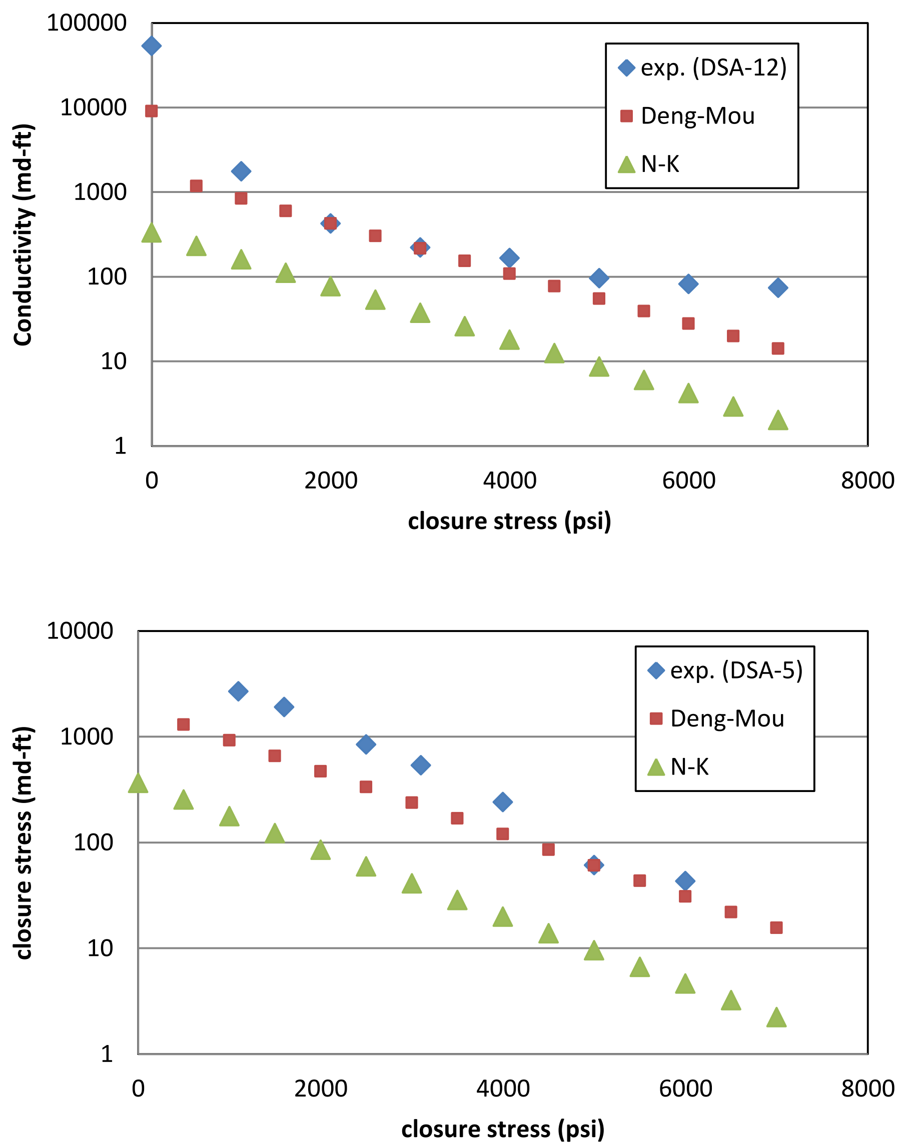


**Figure 52: Comparison between experimental results vs. the N-K and Deng-Mou correlations for conductivity of rough-surface cores**

The discrepancy between the experimental results and the N-K correlation predications might be due to the following reasons:

- N-K does not allow for acid to leak into cores.
- N-K estimates the volume of rock etched using a different technique in which the core weight was measured before and after etching and divided by the change in mass by the rock density.

The only exception was conductivity generated by crosslinked acid that showed a good match with the N-K correlation (Fig. 53). This condition is possibly because the volume etched by crosslinked acid is mainly from the surface, which makes it close to the volume estimated by the N-K correlation method.

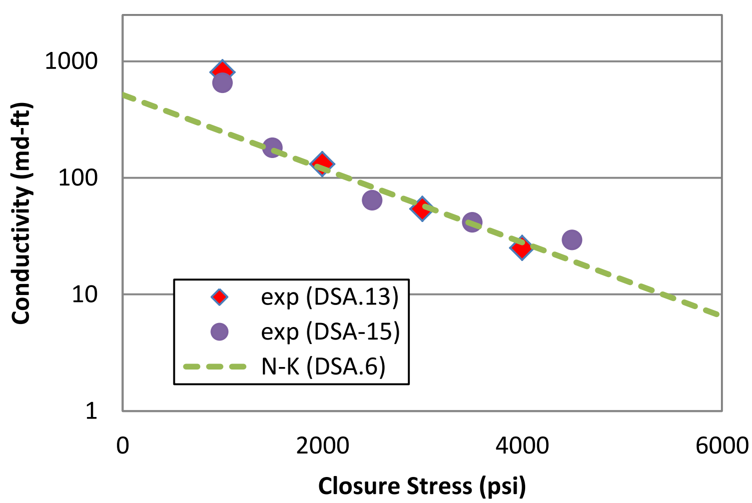


**Figure 53:Comparison between experimental results vs. N-K correlation for cores etched with crosslinked acid**

Generally, there is a tendency for the N-K correlation to underestimate conductivity of rough-surface fractures and the less the volume etched, the more pronounced is the underestimation.

# 4 CONCLUSIONS AND RECOMMENDATIONS

## 4.1 Conclusion

The effects that initial conditions of fracture surfaces have on etched volume, etching pattern, and conductivity have been investigated. The results are summarized below:

- The volume of rock etched on a rough-surface fracture was greater than on a smooth-surface fracture.
- Acid creates conductivity on a rough-surface fracture in a different pattern compared with a smooth-surface fracture.
- The rough-surface fracture showed higher conductivity compared with a smooth-surface fracture etched under the same conditions. The difference between the two is one order of magnitude at low-closure stress. As closure stress increased over 4,000 psi, both conditions converge to the same conductivity values.

The effect acid spending has on the etched volume and the etching pattern on conductivity has been evaluated. The following conclusions can be made:

- Conductivity measurements suggest that increased spending does not automatically reduce conductivity. This finding contradicts previous studies reported in the literature that always assume lower conductivity with an increased in acid spending.
- Etched volume alone is not adequate to predict conductivity. Conductivity is the result of a combination of etching pattern, etched volume, and rock compressive strength after etching.

The investigation of the effect of treatment temperature, acid system type, and contact time showed the following:

- Crosslinked acid etched more rock volume compared with linear-gelled acid at both treatment temperatures.
- The etching patterns were different for each acid type in which gelled acid created additional large pitting compared with crosslinked acid.
- Crosslinked acid is more effective than linear-gelled acid in controlling acid leakoff.

- For a rough-surface fracture, a shorter contact time created high conductivity compared with longer contact time while injecting the same volume of acid.

Comparing experimental results with the N-K and Deng-Mou correlations showed:

- There is a tendency for the N-K correlation to underestimate conductivity of rough- surface fractures and the less the volume etched, the more pronounced is the underestimation.
- Conductivity results of rough-surface fractures showed that an increase in etched volume does not always translate into higher conductivity. One of the shortcomings of the N-K correlation is that it always assumes higher conductivity for higher etched volume given the same rock embedment strength.
- The Deng-Mou correlation better predicts conductivity of rough-surface fractures compared with the N-K correlation.

### 4.2 Recommendations for Future Work

Investigation results for determining the effect fracture surface initial conditions have on conductivity showed that rough-surface fractures predict conductivity differently when compared with smooth-surface fractures. It is desirable to generate a new correlation based on experimental results of rough-surface fractures. Also, comprehensive representation of rock mechanical strength such as Young's modulus should be considered rather than localized RES when correlating conductivity with closure stress and etched volume.

To improve the reliability of laboratory conditions, actual reservoir rocks should be used because they have the same petrophysical properties of the reservoir. Also, cores should be saturated with actual reservoir fluids rather than tap water.

The effect acid spending has on conductivity been examined only for San Andres dolomite using linear-gelled acid. Other types of rock etched with different acid system might experience different behavior. Additional formations and acid systems should be tested to obtain a better insight concerning acid spending effects on conductivity.

One of the shortcomings of the current experimental setup is the high-failure rate due to the deficiency in controlling the leak between the cell body and the core sample polymer sealant. A new design should be considered to mitigate this problem.

# REFERENCES


Abass, H.H., Al-Mulhem, A.A., and Mirajuddin, K.R. 2006. Acid Fracturing or Proppant Fracturing in Carbonate Formation? A Rock Mechanic's View. Paper SPE 102590 presented at the SPE Annual Technical Conference and Exhibition, San Antonio, Texas, 24-27 September.

Anderson, M. S. 1991. Reactivity of San Andres Dolomite. SPE Production Engineering 6 (2): 227-232. SPE 20115.

Anderson, M.S., and Fredrickson, S.E. 1989. Dynamic Etching Tests Aid Fracture-Acidizing Treatment Design. SPE Production Engineering 4 (4): 443-449. SPE 16452.

Antelo, L. F., Pournik, M., Zhu, D., et al. 2009. Surface Characterization and its Effect on Fracture Conductivity in Acid Fracturing. Paper SPE 119743 presented at the SPE Hydraulic Fracturing Technology Conference, The Woodlands, Texas, 19-21 January.

Barron, A. N., Hendrickson, A. R., Wieland, D. R. et. 1962. The Effect of Flow on Acid Reactivity in a Carbonate Fracture. J. Pet Tech. 14 (4):443.-449. SPE-134

Beg, M. S., Kunak, A. O., Gong, M. et al. 1996. A Systematic Experimental Study of Acid Fracture Conductivity. Paper SPE 31098 presented at the SPE International Symposium on Formation Damage Control, Lafayette, Louisiana, 14-15 February.

Crowe, C. W., Martin, R. C., and Michaelis, A. M. 1981. Evaluation of Acid-Gelling Agents for Use in Well Stimulation. Society of Petroleum Engineers Journal 21(4): 415-424. SPE-9384.

Deng, J., Mou, Jianye., Hill, A. D. et al. 2012. A New Correlation of Acid-Fracture Conductivity Subject to Closure Stress. SPE Production & Operation 27 (2). 158-169. SPE-140402.

de Rozieres, J. 1994. Measuring Diffusion Coefficients in Acid Fracturing Fluids and Their Application to Gelled and Emulsified Acids. Paper SPE 28552 presented at the

SPE Annual Technical Conference and Exhibition, New Orleans, Louisiana, 25-28 September

Economides, M.J., Hill, A.D., and Ehlig-Economides, C. 1994. *Petroleum Production Systems*. New Jersey: Prentice Hall Petroleum Engineering Series.

Gong, M., Lacote, S., and Hill, A.D. 1998. New Model of Acid-Fracture Conductivity Based on Deformation of Surface Asperities. Paper SPE 39431 presented at the SPE International Formation Damage Symposium, Lafayette, Louisiana, 18-19 February.

Malagon, C. 2006. The Texture of Acidized Fracture Surfaces-Implications for Acid Fracture Conductivity. MS thesis, Texas A&M U., College Station, Texas (May 2006).

Melendez, M.G. 2007. The Effects of Acid Contact Time and Rock Surfaces on Acid Fracture Conductivity. MS thesis, Texas A&M U., College Station, Texas (August 2007).

Malik, M. A. and Hill, A. D. 1989. A New Technique for Laboratory Measurement of Acid Fracture Conductivity. Paper SPE 19733 presented at the SPE Annual Technical Conference and Exhibition, San Antonio, Texas, 8-11 October.

Mumallah, N.M. 1991. Factors Influencing the Reaction Rate of Hydrochloric Acid and Carbonate Rock. Paper SPE 21036 presented at the SPE International Symposium on Oilfield Chemistry, Anaheim, California, 20-22 February.

Nasr-El-Din, H.A., Al-Driweesh, S. M., Metcalf, A. S., et al. 2006. Fracture Acidizing: What Role Does Formation Softening Play in Production Response?. Paper SPE 103344 presented at the SPE Annual Technical Conference and Exhibition, San Antonio, Texas, 24-27 September.

Neumann, L. F., Oliveira, T. J. L., and Fernandes, P. D. 2012. Building Acid Frac Conductivity in Highly-Confined Carbonates. Paper SPE 152164 presented at the SPE Hydraulic Fracturing Technology Conference, The Woodlands, Texas, 6-8 February

Neumann, L. F., de Oliveira e Sousa, J. L. A. O., and Oliveira, T. J. L. 2012. Acid Fracturing: New Insigths on Acid Etching Patterns from Experimental Investigation.

Paper SPE 152179 presented at the SPE Hydraulic Fracturing Technology Conference, The Woodlands, Texas, 6-8 February

Nierode, D.E., and Kruk, K.F. 1973. An Evaluation of Acid Fluid Loss Additives, Retarded Acids, and Acidized Fracture Conductivity. Paper SPE 4549 presented at the Annual Fall Meeting, Las Vegas, Nevada, 30 September–3 October.

Nierode, D. E., Williams, B. R. and Bombardieri, C. C. 1972. Prediction of Stimulation From Acid Fracturing Treatments. Journal of Canadian Petroleum Technology 11 (4). 31-41. SPE-72-04-04

Novotny, E. J. 1977. Prediction of Stimulation From Acid Fracturing Treatments Using Finite Fracture Conductivity. Journal of Petroleum Technology 29 (9): 1186-1194. SPE-6123.

Pongthunya, P. 2007. Development, Setup and Testing of a Dynamic Hydraulic Fracture Conductivity Apparatus. MS thesis, Texas A&M U., College Station, Texas (August 2007).

Pournik, M. 2008. Laboratory-Scale Fracture Conductivity Created by Acid Etching. PhD dissertation, Texas A&M U., College Station, Texas (December 2008).

Van Domelen, M.S. 1992. Optimizing Fracture Acidizing Treatment Design by Integrating Core Testing, Field Testing, and Computer Simulation. Paper SPE 22393 presented at the SPE International Meeting on Petroleum Engineering, Beijing, China, 24-27 March.

Van Domelen, M.S., Gdanski, R.D., Finley, D.B. 1994. The Application of Core and Well Testing to Fracture Acidizing Treatment Design: A Case Study. Paper SPE 27621 presented at the European Production Operations Conference and Exhibition, Aberdeen, U.K., 15-17 March.

Walsh, J.B. 1981. Effect of Pore Pressure and Confining Pressure on Fracture Permeability. International Journal of Rock Mechanics and Mining Sciences & Geomechanics Abstracts. 18 (5):429-435.

# APPENDIX

**Given:**

- **12 liter of 15% wt HCl acid.**

**Wanted:**

- **If 50 % of acid reacted with dolomite rock what will be the ions concentration of the products in the spent acid?**

Density of 15 wt% HCl= 1.0725 g/ml

Volume of 15 wt% HCl acid= 12000 ml

Mass of Solution= =M=ρ*V=1.0725 *12000=12870 gm

Mass of HCl in 15 %wt HCl solution =0.15*12870=1930.5 gm

**Assuming that the acid will only react with dolomite**: if 50% of original (15 % wt HCl) acid reacted then the mass of acid reacted will be = 1930.5 *0.5=965.25 gm.

We need to convert the mass to mole

MW of HCl= 36.46 gm/mole (H=1.008, Cl=35.45)

Conversion from gram to mole

965.25 gam* (1 mole/36.45 gm)= 26.48 mole of HCl

From the stoichiometry of reaction of HCl with dolomite:

$$\boldsymbol{4HCl + CaMg(CO_3)_2 \rightarrow CaCl_2 + MgCl_2 + 2H_2O + 2CO_2}$$

To determine the no mole of CaCl2 and MgCl2 that will be produced we use this ratio (4HCL mole/1CaCl2 mole) and (4HCL mole/1MgCl2 mole)

So, 26.48 mole of HCl *(4HCL mole/1CaCl2 mole) = 26.48/4= 6.62 mole of CaCl2

The same thing applies to MgCl2=6.62 mole

Now we need to convert mole to gram. To do this we need molecular weight of both compounds

MW(CaCl2)=40.48+ 2*35.45=110.98 gm/mole

MW(MgCl2)=24.31+ 2*35.45=95.21 gm/mole

**Mass of MgCl2=6.62 mole *95.21 gm/mole=630.29 gm**

**Mass of CaCl2=6.62 mole *110.98 gm/mole=734.69 gm**

| Experiment. 2 | |
|---|---|
| **Sample No.** | DSA_2 |
| **Rock Type** | San Andres Dolomite |
| **Acid Type** | Gelled Acid |
| **Date** | 6/4/2012 |

| Test Condition | | |
|---|---|---|
| **Q (0.5 liter/min) @ 1000 psi** | 0.434783 | l/min |
| **Contact Time** | 20 | min |
| **Temperature (F)** | 130 | F |

| Acid Preparation & Measurements | | |
|---|---|---|
| **Formula** | DG315: 4.5% J429 (4.5% Polymer) | |
| **Volume** | 12 | L |
| **H2O** | 3515.35 | Ml |
| **A262 (Corrosion Inhibitor)** | 36 | Ml |
| **1058 (Iron Stabilizer)** | 14.37 | Mg |
| **HCl (28%)** | 4393.3 | Ml |
| **H2O** | 3515.35 | Ml |
| **J429** | 540 | Ml |

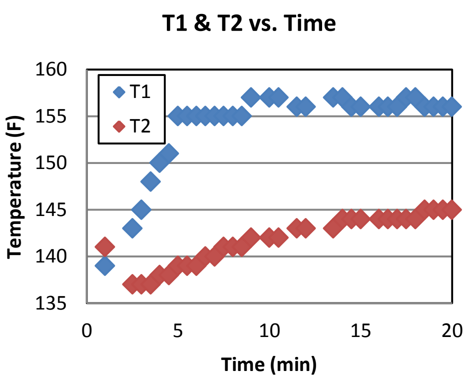


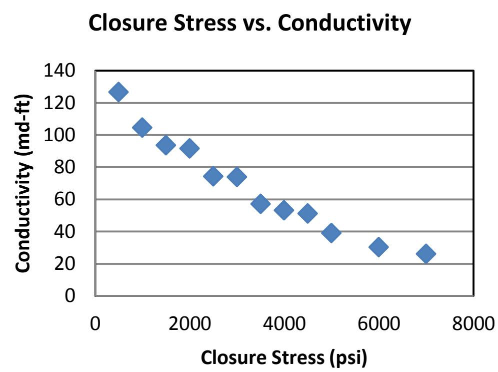


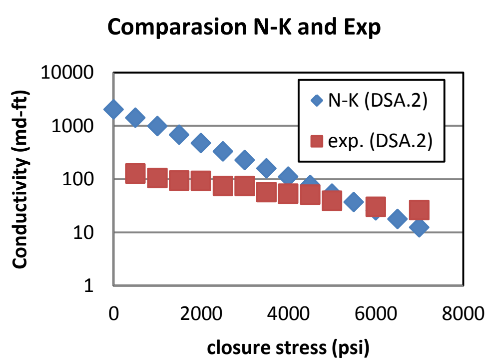


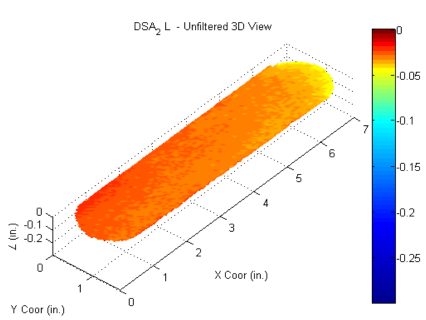


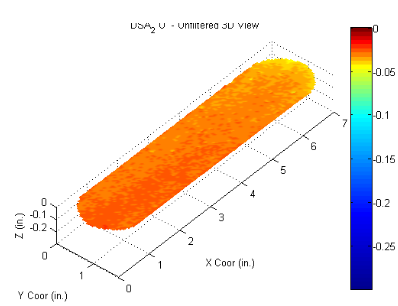

| Experiment. DSA-3 | |
|---|---|
| **Sample No.** | DSA_3 |
| **Rock Type** | San Andres Dolomite |
| **Acid Type** | Gelled Acid |
| **Date** | 6/6/2012 |

| Test Condition | | |
|---|---|---|
| **Q (1 liter/min) @ 1000 psi** | 0.84507 | l/min |
| **Contact Time** | 10 | min |
| **Temperature (F)** | 130 | F |

| Acid Preparation & Measurements | | |
|---|---|---|
| **Formula** | DG315: 4.5% J429 (4.5% Polymer) | |
| **Volume** | 12 | L |
| **H2O** | 3515.35 | Ml |
| **A262 (Corrosion Inhibitor)** | 36 | Ml |
| **1058 (Iron Stabilizer)** | 14.37 | Mg |
| **HCl (28%)** | 4393.3 | Ml |
| **H2O** | 3515.35 | Ml |
| **J429** | 540 | Ml |

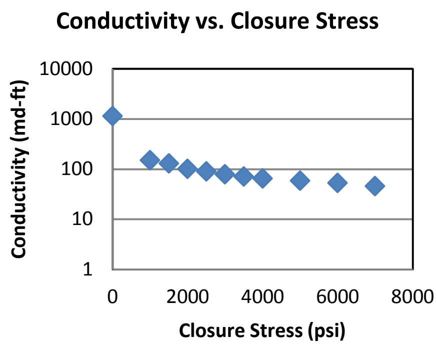


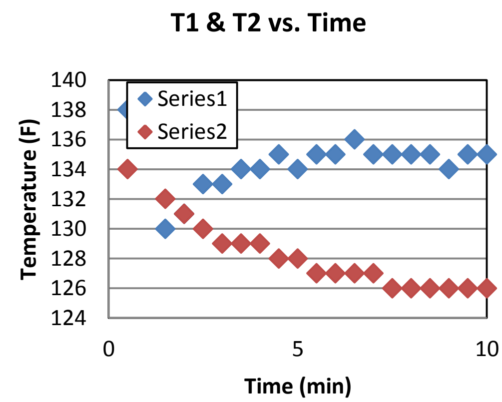


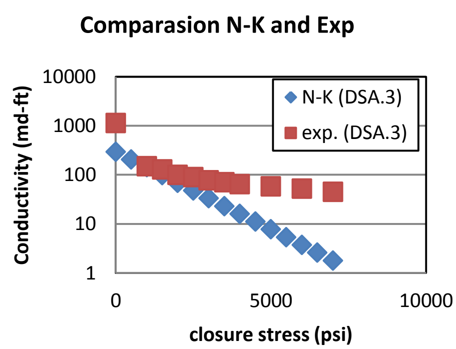


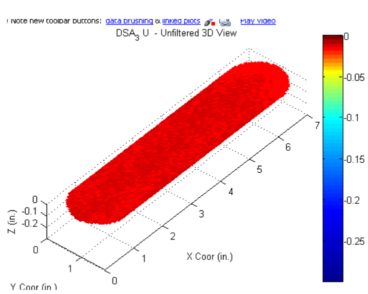


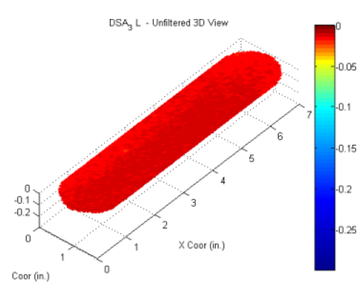

| Experiment. 4 | |
|---|---|
| **Sample No.** | DSA_4 |
| **Rock Type** | San Andres Dolomite |
| **Acid Type** | Gelled Acid |
| **Date** | 10/5/2012 |

| Test Condition | | |
|---|---|---|
| **Q (0.5 liter/min) @ 1000 psi** | 0.416667 | l/min |
| **Contact Time** | 20 | min |
| **Temperature (F)** | 130 | F |

| Acid Preparation & Measurements | | |
|---|---|---|
| **Formula** | DG315: 4.5% J429 (4.5% Polymer) | |
| **Volume** | 12 | L |
| **H2O** | 3515.35 | Ml |
| **A262 (Corrosion Inhibitor)** | 36 | Ml |
| **1058 (Iron Stabilizer)** | 14.37 | Mg |
| **HCl (28%)** | 4393.3 | Ml |
| **H2O** | 3515.35 | Ml |
| **J429** | 540 | Ml |

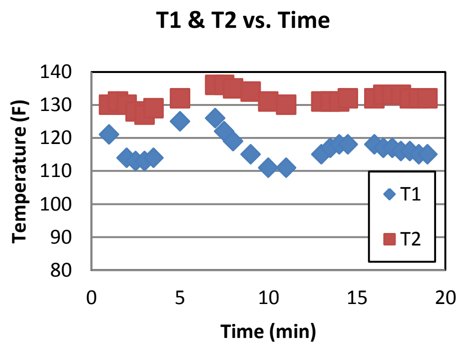


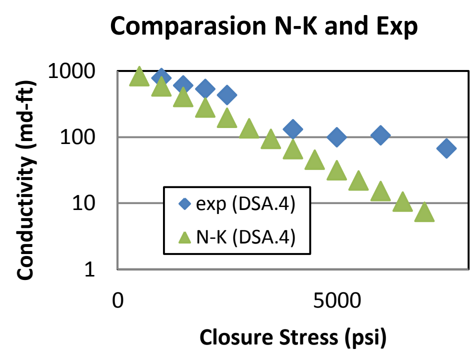


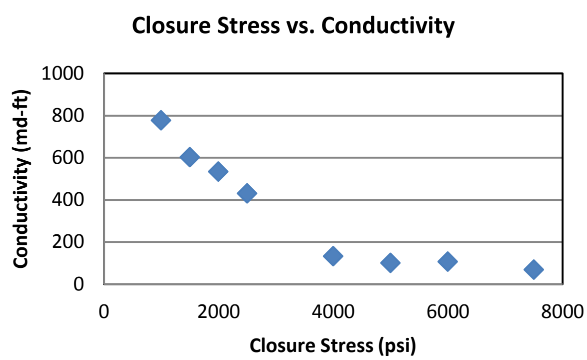


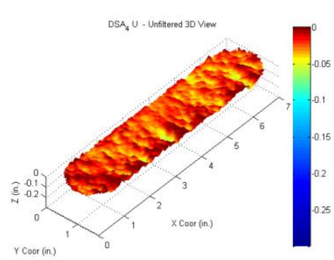

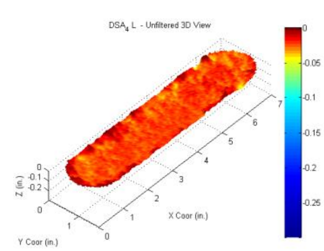

| Experiment. 5 | |
|---|---|
| Sample No. | DSA_5 |
| Rock Type | San Andres Dolomite |
| Acid Type | Gelled Acid |
| Date | 9/21/2012 |

| Test Condition | | |
|---|---|---|
| Q (1 liter/min) @ 1000 psi | 0.857143 | l/min |
| Contact Time | 10 | min |
| Temperature (F) | 130 | F |

| Acid Preparation & Measurements | | |
|---|---|---|
| Formula | DG315: 4.5% J429 (4.5% Polymer) | |
| Volume | 12 | L |
| H2O | 3515.35 | Ml |
| A262 (Corrosion Inhibitor) | 36 | Ml |
| 1058 (Iron Stabilizer) | 14.37 | Mg |
| HCl (28%) | 4393.3 | Ml |
| H2O | 3515.35 | Ml |
| J429 | 540 | Ml |

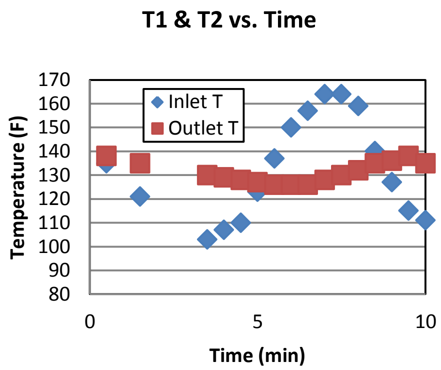


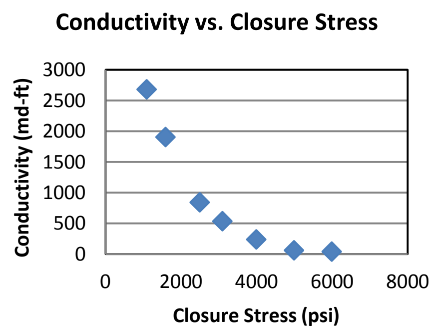


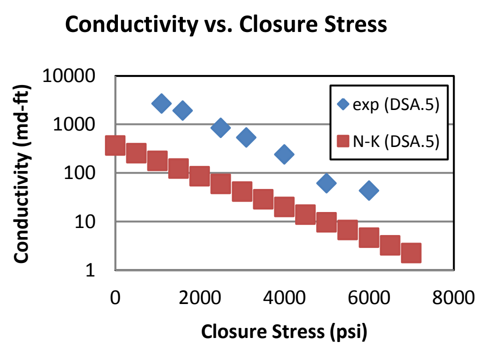


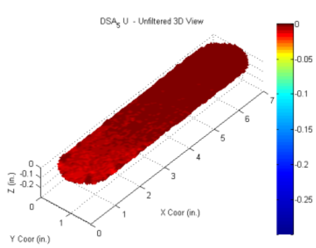

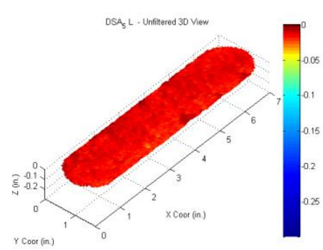

| Experiment. 6 | |
|---|---|
| Sample No. | DSA_6 |
| Rock Type | San Andres Dolomite |
| Acid Type | Gelled Acid |
| Date | 11/2/2012 |

| Test Condition | | |
|---|---|---|
| Q (0.5 liter/min) @ 1000 psi | 0.983607 | l/min |
| Contact Time | 10 | min |
| Temperature (F) | 130 | F |

| Acid Preparation & Measurements | | |
|---|---|---|
| Formula | DG315: 4.5% J429 (4.5% Polymer) | |
| Volume | 12 | L |
| H2O | 3515.35 | Ml |
| A262 (Corrosion Inhibitor) | 36 | Ml |
| 1058 (Iron Stabilizer) | 14.37 | Mg |
| HCl (28%) | 4393.3 | Ml |
| H2O | 3515.35 | Ml |
| J429 | 540 | Ml |

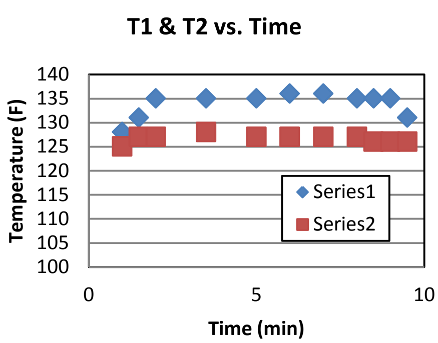


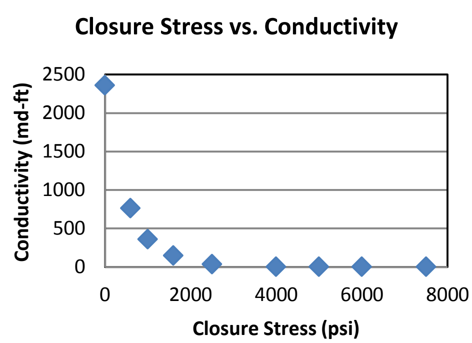


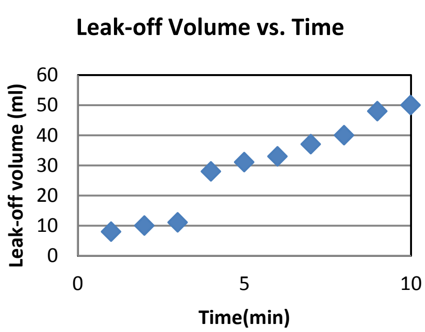


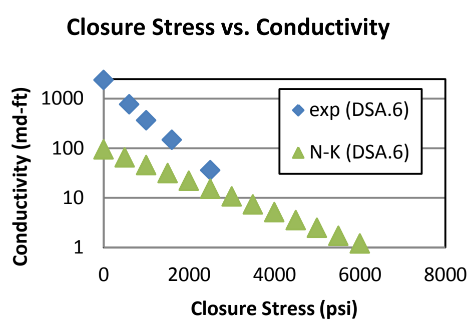


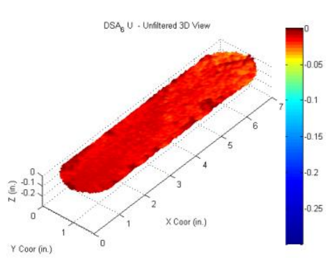

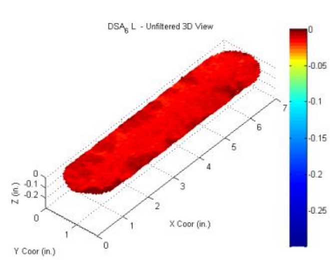

| Experiment. 7 | |
|---|---|
| **Sample No.** | DSA_7 |
| **Rock Type** | San Andres Dolomite |
| **Acid Type** | Gelled Acid |
| **Date** | 11/15/2012 |

| Test Condition | | |
|---|---|---|
| **Q (0.5 liter/min) @ 1000 psi** | 0.475 | l/min |
| **Contact Time** | 20 | min |
| **Temperature (F)** | 130 | F |

| Acid Preparation & Measurements | | |
|---|---|---|
| **Formula** | DG315: 4.5% J429 (4.5% Polymer) | |
| **Volume** | 12 | L |
| **H2O** | 3515.35 | Ml |
| **A262 (Corrosion Inhibitor)** | 36 | Ml |
| **1058 (Iron Stabilizer)** | 14.37 | Mg |
| **HCl (28%)** | 4393.3 | Ml |
| **H2O** | 3515.35 | Ml |
| **J429** | 540 | Ml |

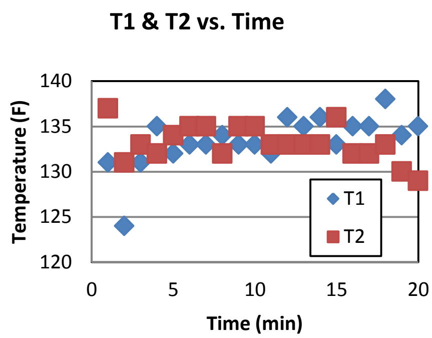


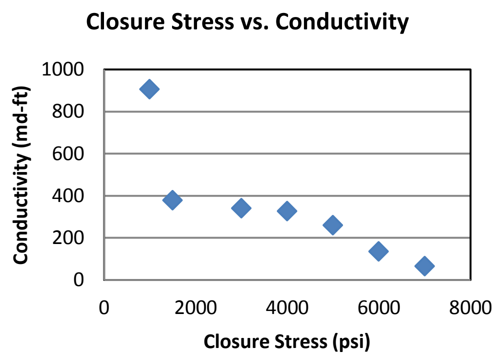


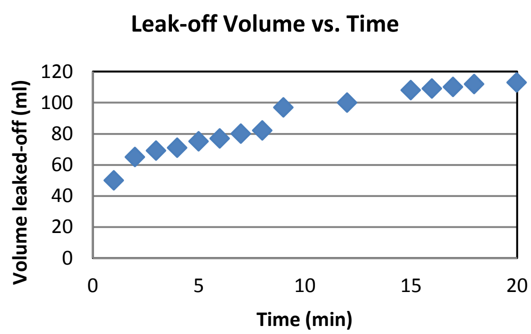

| Experiment. 8 | |
|---|---|
| **Sample No.** | DSA_8 |
| **Rock Type** | San Andres Dolomite |
| **Acid Type** | Gelled Acid |
| **Date** | 12/4/2012 |

| Test Condition | | |
|---|---|---|
| **Q (1.0 liter/min) @ 1000 psi** | 0.895522 | l/min |
| **Contact Time** | 10 | min |
| **Temperature (F)** | 130 | F |

| Acid Preparation & Measurements | | |
|---|---|---|
| **Formula** | DG315: 4.5% J429 (4.5% Polymer) | |
| **Volume** | 12 | L |
| **H2O** | 8267 | Ml |
| **A262 (Corrosion Inhibitor)** | 36 | Ml |
| **1058 (Iron Stabilizer)** | 14.37 | Mg |
| **HCl (28%)** | 2196.7 | Ml |
| **MgCl2.6H2O** | 1350.96 | Gm |
| **CaCl2.2H2O** | 974.39 | Gm |
| **J429** | 540 | Ml |

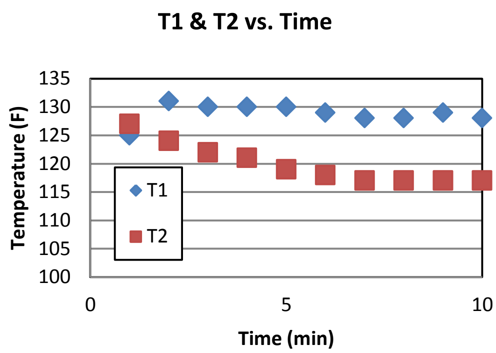


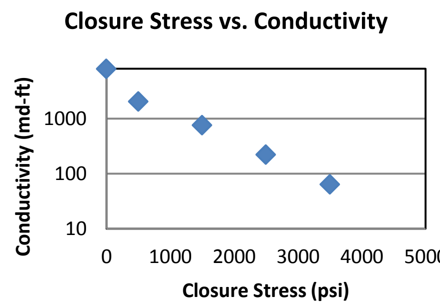


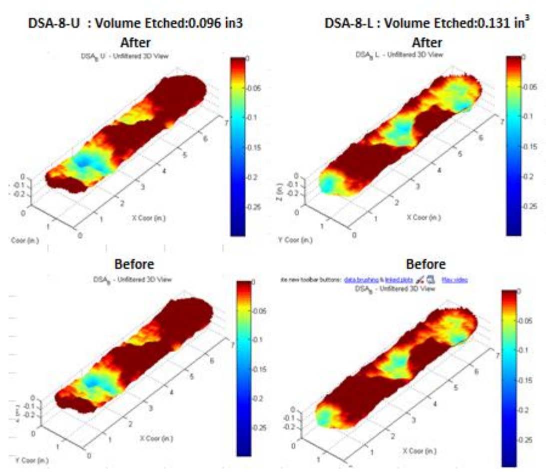


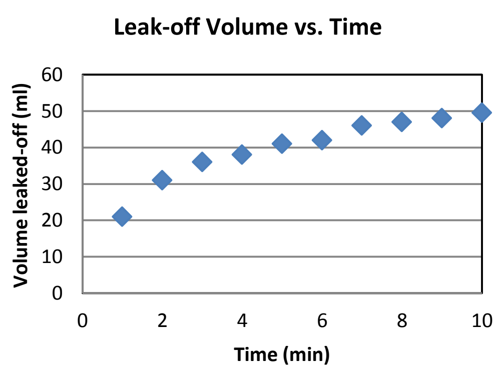

| Experiment. 11 | |
|---|---|
| Sample No. | DSA_11 |
| Rock Type | San Andres Dolomite |
| Acid Type | Gelled Acid |
| Date | 3/6/2013 |

| Test Condition | | |
|---|---|---|
| Q (0.5 liter/min) @ 1000 psi | 0.909091 | l/min |
| Contact Time | 10 | min |
| Temperature (F) | 100 | F |

| Acid Preparation & Measurements | | |
|---|---|---|
| Formula | DG315: 4.5% J429 (4.5% Polymer) | |
| Volume | 12 | L |
| H2O | 3515.35 | Ml |
| A262 (Corrosion Inhibitor) | 36 | Ml |
| 1058 (Iron Stabilizer) | 14.37 | Mg |
| HCl (36%) | 4393.3 | Ml |
| H2O | 3515.35 | Ml |
| J429 | 540 | Ml |

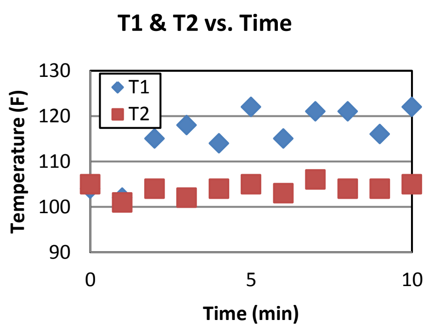


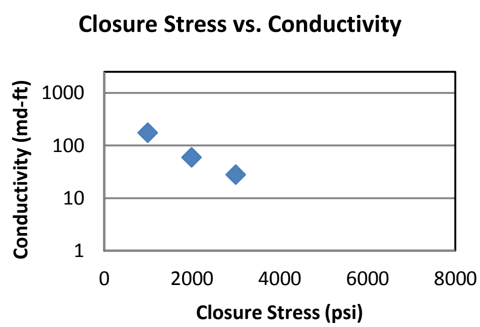


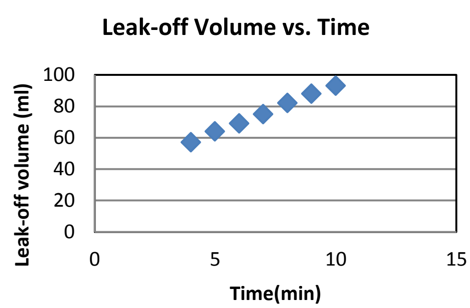


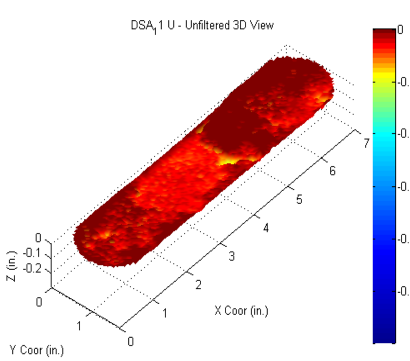


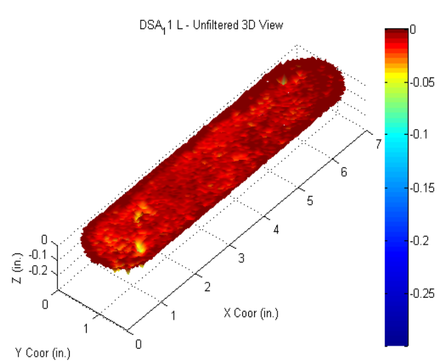

| Experiment. 12 | |
|---|---|
| **Sample No.** | DSA_12 |
| **Rock Type** | San Andres Dolomite |
| **Acid Type** | X-linked Acid |
| **Date** | 3/8/2013 |

| Acid Preparation & Measurements | | |
|---|---|---|
| **Formula** | LCA | |
| **Volume** | 12 | L |
| **H2O** | 6880 | ml |
| **A262 (Corrosion Inhibitor)** | 36 | ml |
| **HCl (36%)** | 4393.3 | ml |
| **J548 (iron control agent)** | 120 | ml |
| **J472 (fluid-loss control)** | 30 | ml |
| **J429 (polymer)** | 540 | ml |

| Test Condition | | |
|---|---|---|
| **Q (0.5 liter/min) @ 1000 psi** | 0.882353 | l/min |
| **Contact Time** | 10 | min |
| **Temperature (F)** | 100 | F |

**T1 & T2 vs. Time**

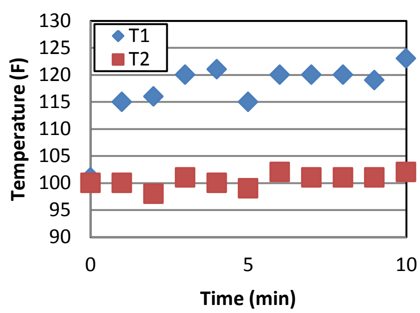


**Closure Stress vs. Conductivity**

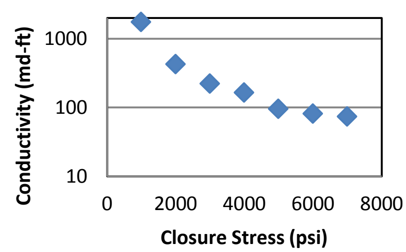


**Leak-off Volume vs. Time**

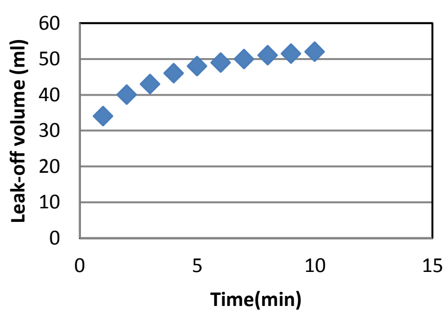


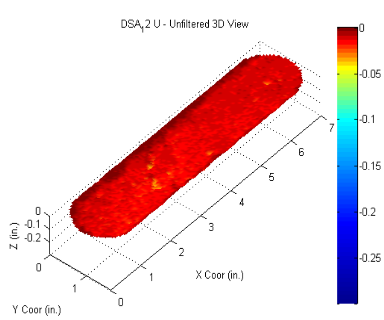


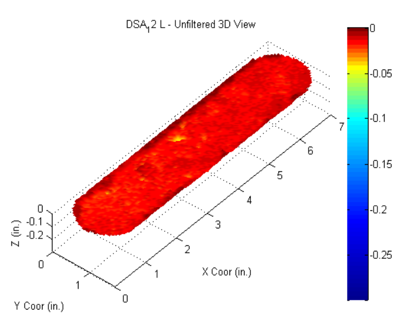

| Experiment. 13 | |
|---|---|
| **Sample No.** | DSA_13 |
| **Rock Type** | San Andres Dolomite |
| **Acid Type** | X-linked Acid |
| **Date** | 3/7/2013 |

| Test Condition | | |
|---|---|---|
| **Q (0.5 liter/min) @ 1000 psi** | 1 | l/min |
| **Contact Time** | 10 | min |
| **Temperature (F)** | 130 | F |

| Acid Preparation & Measurements | | |
|---|---|---|
| **Formula** | LCA | |
| **Volume** | 12 | L |
| **H2O** | 6880 | Ml |
| **A262 (Corrosion Inhibitor)** | 36 | Ml |
| **HCl (36%)** | 4393.3 | Ml |
| **J548 (iron control agent)** | 120 | Ml |
| **J472 (fluid-loss control)** | 30 | Ml |
| **J429 (polymer)** | 540 | Ml |

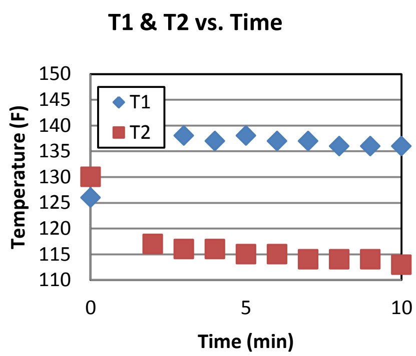


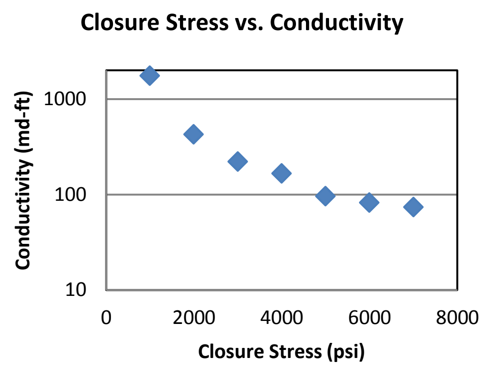


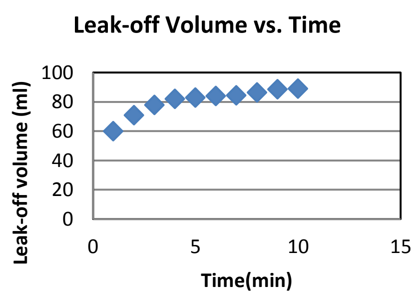


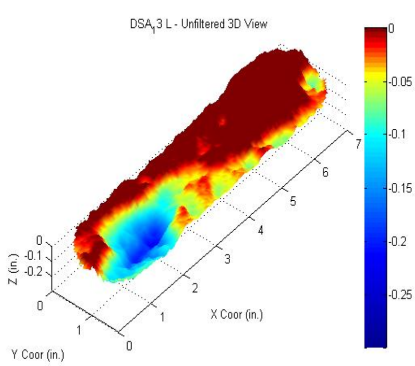


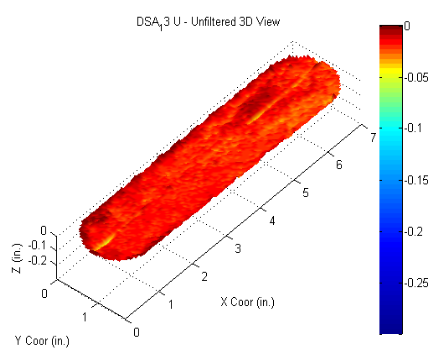

| Experiment. 14 | |
|---|---|
| **Sample No.** | DSA_14 |
| **Rock Type** | San Andres Dolomite |
| **Acid Type** | 90% Spent Gelled Acid |
| **Date** | 3/22/2013 |

| Test Condition | | |
|---|---|---|
| **Q (1.0 liter/min) @ 1000 psi** | 0.923077 | l/min |
| **Contact Time** | 10 | min |
| **Temperature (F)** | 130 | F |

| Acid Preparation & Measurements | | |
|---|---|---|
| **Formula** | DG315: 4.5% J429 (4.5% Polymer) | |
| **Volume** | 12 | L |
| **H2O** | 9274 | Ml |
| **A262 (Corrosion Inhibitor)** | 36 | Ml |
| **1058 (Iron Stabilizer)** | 14.37 | Mg |
| **HCl (36%)** | 425.9 | Ml |
| **MgCl2.6H2O** | 2430.19 | Gm |
| **CaCl2.2H2O** | 1754.4 | Gm |
| **J429** | 540 | Ml |

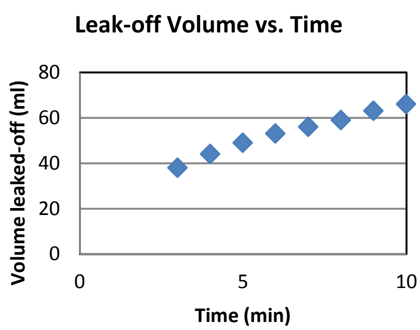


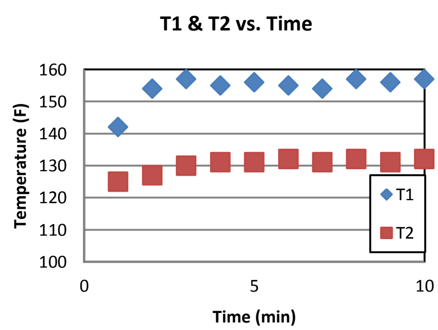


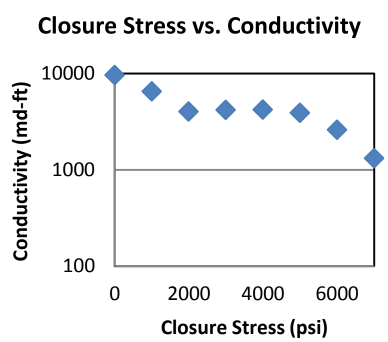


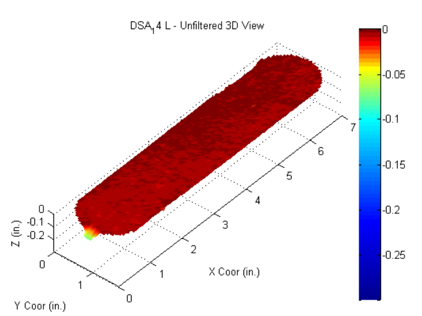


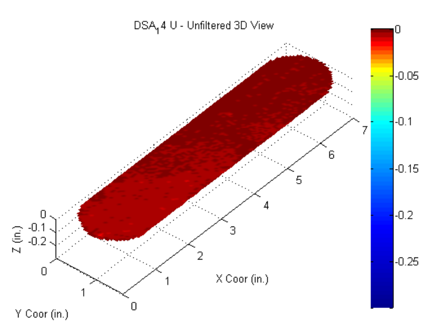

| Experiment. 15 | |
|---|---|
| **Sample No.** | DSA_15 |
| **Rock Type** | San Andres Dolomite |
| **Acid Type** | X-linked Acid |
| **Date** | 4/9/2013 |

| Test Condition | | |
|---|---|---|
| **Q (0.5 liter/min) @ 1000 psi** | 0.967742 | l/min |
| **Contact Time** | 10 | min |
| **Temperature (F)** | 130 | F |

| Acid Preparation & Measurements | | |
|---|---|---|
| **Formula** | LCA | |
| **Volume** | 12 | L |
| **H2O** | 6880 | Ml |
| **A262 (Corrosion Inhibitor)** | 36 | Ml |
| **HCl (36%)** | 4393.3 | Ml |
| **J548 (iron control agent)** | 120 | Ml |
| **J472 (fluid-loss control)** | 30 | Ml |
| **J429 (polymer)** | 540 | Ml |

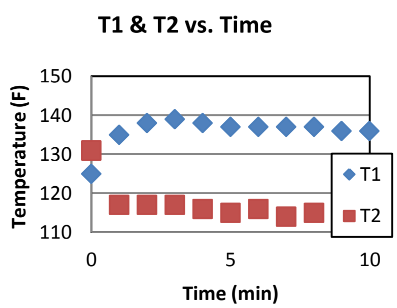


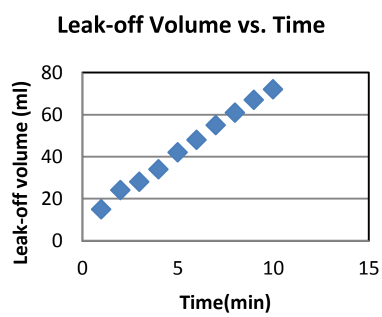


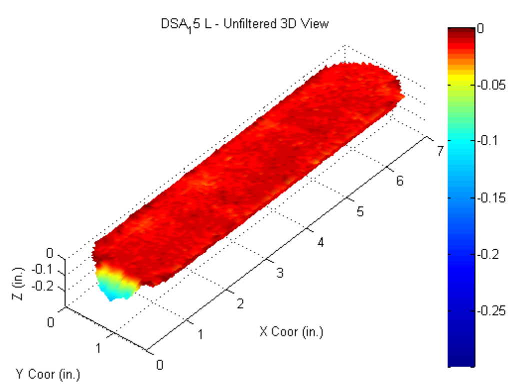


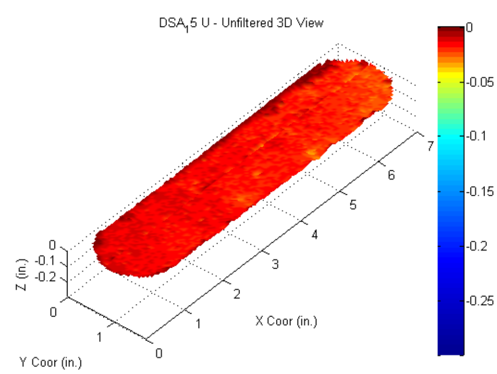

| Experiment. 16 | |
|---|---|
| **Sample No.** | DSA_16 |
| **Rock Type** | San Andres Dolomite |
| **Acid Type** | 90% Spent Gelled Acid |
| **Date** | 4/13/2013 |

| Test Condition | | |
|---|---|---|
| **Q (1.0 liter/min) @ 1000 psi** | 0.909091 | l/min |
| **Contact Time** | 10 | min |
| **Temperature (F)** | 130 | F |

| Acid Preparation & Measurements | | |
|---|---|---|
| **Formula** | DG315: 4.5% J429 (4.5% Polymer) | |
| **Volume** | 12 | L |
| **H2O** | 9274 | Ml |
| **A262 (Corrosion Inhibitor)** | 36 | Ml |
| **1058 (Iron Stabilizer)** | 14.37 | Mg |
| **HCl (36%)** | 425.9 | Ml |
| **MgCl2.6H2O** | 2430.19 | Gm |
| **CaCl2.2H2O** | 1754.4 | Gm |
| **J429** | 540 | Ml |

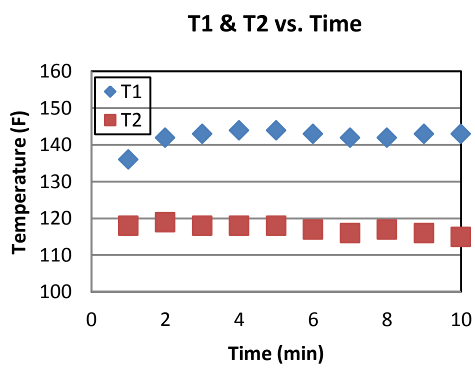


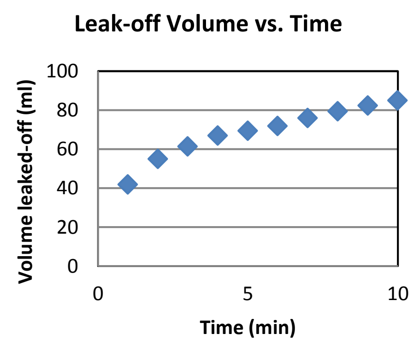


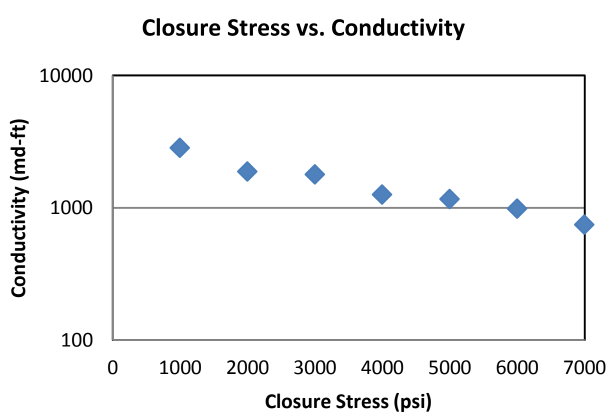

| Experiment. 17 | |
|---|---|
| Sample No. | DSA_17 |
| Rock Type | San Andres Dolomite |
| Acid Type | Gelled Acid |
| Date | 3/26/2013 |

| Test Condition | | |
|---|---|---|
| Q (0.5 liter/min) @ 1000 psi | 0.82 | l/min |
| Contact Time | 10 | min |
| Temperature (F) | 100 | F |

| Acid Preparation & Measurements | | |
|---|---|---|
| Formula | DG315: 4.5% J429 (4.5% Polymer) | |
| Volume | 12 | L |
| H2O | 3515.35 | Ml |
| A262 (Corrosion Inhibitor) | 36 | Ml |
| 1058 (Iron Stabilizer) | 14.37 | Mg |
| HCl (36%) | 4393.3 | Ml |
| H2O | 3515.35 | Ml |
| J429 | 540 | Ml |

T1 & T2 vs. Time

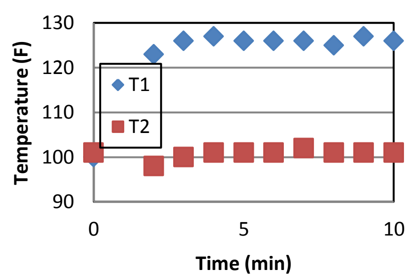


Closure Stress vs. Conductivity

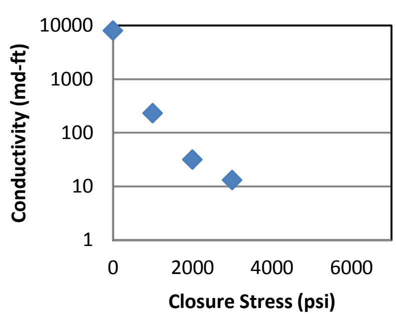


Leak-off Volume vs. Time

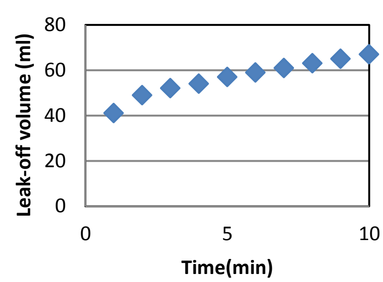


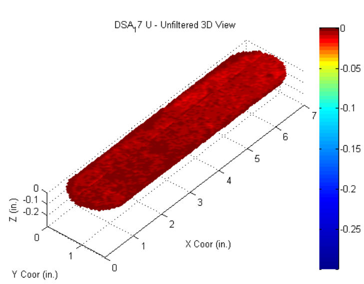

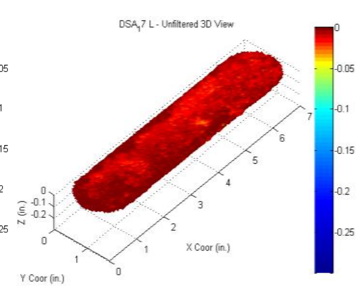

| Volume Etched vs. Temp. All Conditions | | | | |
|---|---|---|---|---|
| **Sample** | **Contact Time** | **Etched Vol.** | **Avg T in** | **Avg T out** |
| **No.** | **min** | **in3** | **F** | **F** |
| DSA-2 (smooth) | 20 | 0.31 | 154.09 | 141.72 |
| DSA-3 (smooth) | 10 | 0.143 | 134.32 | 128.11 |
| DSA-4 | 20 | 0.226 | 117.11 | 132.37 |
| DSA-5 | 10 | 0.155 | 132.69 | 131.19 |
| DSA-6 | 10 | 0.152 | 133.82 | 126.64 |
| DSA-8 (half spent) | 10 | 0.096 | 128.80 | 119.90 |
| DSA-11 | 10 | 0.065 | 115.45 | 103.91 |
| DSA-12 (X-linked) | 10 | 0.149 | 117.27 | 100.45 |
| DSA-13 (X-linked) | 10 | 0.178 | 135.90 | 116.40 |
| DSA-14 (90% spent) | 10 | 0.054 | 154.30 | 130.20 |
| DSA-15 (X-linked) | 10 | 0.17 | 137.00 | 115.70 |
| DSA-17 | 10 | 0.069 | 123.20 | 100.70 |

| Volume Etched of Smooth vs. Rough-walled Surface at 130 F | | | | |
|---|---|---|---|---|
| **Sample** | **Contact Time** | **Etched Vol.** | **Avg T in** | **Avg T out** |
| **No.** | **min** | **in3** | **F** | **F** |
| DSA-3 (smooth) | 10 | 0.143 | 134.32 | 128.1 |
| DSA-5 (rough) | 10 | 0.155 | 132.69 | 131.18 |

| Volume Etched of X-linked vs. Linear Gelled at 100 and 130 F | | | | |
|---|---|---|---|---|
| **Sample** | **Contact Time** | **Etched Vol.** | **Avg T in** | **Avg T out** |
| **No.** | **min** | **in3** | **F** | **F** |
| DSA-12 (X-linked) | 10 | 0.149 | 117.27 | 100.45 |
| DSA-13 (X-linked) | 10 | 0.178 | 135.90 | 116.40 |
| DSA-11 | 10 | 0.065 | 115.45 | 103.91 |
| DSA-5 | 10 | 0.155 | 132.69 | 131.19 |

| Volume Etched vs. Acid Spending | | | | |
|---|---|---|---|---|
| **Sample** | **Contact Time** | **Etched Vol.** | **Avg T in** | **Avg T out** |
| **No.** | **min** | **in3** | **F** | **F** |
| DSA-5 (base-line) | 10 | 0.155 | 132.69 | 131.19 |
| DSA-8 (half spent) | 10 | 0.096 | 128.80 | 119.90 |
| DSA-14 (90% spent) | 10 | 0.054 | 154.30 | 130.20 |

**Comparison of etched volume of this study with Melendez 2007**

| Variable | Temperature | Contact Time | Etched Volume |
|---|---|---|---|
| | F | min | $in^3$ |
| Melendez | 175 | 10 | 0.19 |
| | 175 | 20 | 0.32 |
| | 175 | 30 | 0.47 |
| This Study | 130 | 10 | 0.155 |
| | 130 | 20 | 0.226 |